Modelling of bed sediment composition changes at the lower shoreface of the Sand Motor

Huisman, B. J.A.; Ruessink, B. G.; de Schipper, M. A.; Luijendijk, A. P.; Stive, M. J.F.

DOI
10.1016/j.coastaleng.2017.11.007

Publication date
2018

Document Version
Accepted author manuscript

Published in
Coastal Engineering

Citation (APA)
Huisman, B. J. A., Ruessink, B. G., de Schipper, M. A., Luijendijk, A. P., & Stive, M. J. F. (2018). Modelling of bed sediment composition changes at the lower shoreface of the Sand Motor. *Coastal Engineering*, *132*, 33-49. https://doi.org/10.1016/j.coastaleng.2017.11.007

Modelling of bed sediment composition changes at the lower shoreface of the Sand Motor

B.J.A. Huisman[a,b,*], B.G. Ruessink[c], M.A. de Schipper[a,d], A.P. Luijendijk[a,b], M.J.F. Stive[a]

[a] *Delft University of Technology, Faculty of Civil Engineering and Geosciences, Department of Hydraulic Engineering, P.O. Box 5048, 2600GA, Delft, The Netherlands*
[b] *Deltares, Unit Hydraulic Engineering, Department of Harbour, Coastal and Offshore Engineering, P.O. Box 177, 2600MH, Delft, The Netherlands*
[c] *Utrecht University, Faculty of Geosciences, Department of Physical Geography, P.O. Box 80115, 3508TC Utrecht, The Netherlands*
[d] *Shore Monitoring and Research, P.O. Box 84070, 2508AB, The Hague, The Netherlands*

Abstract

Large perturbations in the coastline, such as the 'Sand Motor' nourishment (∼21 million m^3) at the Holland coast, can initiate considerable spatial and temporal changes in the median grain size (D_{50}) of the sea bed on the lower shoreface. The relevance of hydrodynamic conditions for the development of the heterogeneity in D_{50} at large-scale nourishments was assessed with a numerical model (Delft3D), which required a validation against 2.5 years of D_{50} measurements. A good representation of the observed spatial pattern of D_{50} was obtained independent of a 2DH or 3D approach and initial condition for the D_{50} of the bed. Five sediment size fractions and a multi-layer administration of the bed composition were used. The extent and magnitude of the coarsening of the bed is related to the velocity of the horizontal tide, while a far less pronounced coarsening takes place during energetic conditions (i.e. $H_{m0} \geq 3$ m). Differential suspension behaviour between the size fractions, which are all mobilized at the bed, causes a preferential transport of fine sediment (in alongshore direction) away from the Sand Motor at the lower shoreface (i.e. seaward of MSL -6m). Storm conditions may induce a partial removal of the coarse top-layer due to mobilization of all of the size fractions and mixing with the relatively fine substrate material. Simulations also show that transport of the fine sand fraction extents to much deeper water than for the medium and coarse sand fractions. Models with multiple sediment fractions are therefore required for the assessment of environmental impacts of large-scale coastal structures or land reclamation's and sediment transport on the lower shoreface.

Keywords: Nourishment, Bed sediment, Sorting, Grain size, Numerical modelling

1. Introduction

Spatial heterogeneity of bed sediment composition is observed at many coasts around the world (Holland and Elmore, 2008), but seldom accounted for in morphological or environmental impact studies of coastal interventions (e.g. modelling of sand nourishments; Capobianco et al., 2002). Knowledge of the potential spatial variability of the bed sediment (i.e. grain size and grading) is however considered essential for the understanding of the ecological impact of large-scale coastal interventions. Firstly, bed composition changes affect the ecological habitats for benthic species

*Corresponding author

and fish (e.g. McLachlan, 1996; Knaapen et al., 2003). Small changes in the top-layer grain size can, for example, significantly affect the burrowing ability of juvenile plaice (Gibson and Robb, 1992). Secondly, long-term morphological changes can be affected by bed coarsening when preferential transport of finer sand fractions takes place at large-scale sand nourishments (Van Rijn, 2007b), which is especially relevant for the region outside the surfzone (Huisman et al., 2016).

Spatial heterogeneity of the bed composition of natural coasts is characterized by a fining of sediment grain size in the offshore direction with coarsest sediment being found in the swash zone (Inman, 1953; Sonu, 1972; Liu and Zarillo, 1987; Pruszak, 1993; Horn, 1993; Stauble and Cialone, 1996; Kana et al., 2011). In the presence of sub-tidal bars the spatial pattern of the bed sediment composition can vary between different studies. Generally, coarser sediment is observed in the bar troughs and finer sediment on bar crests (Moutzouris et al., 1991; Katoh and Yanagishima, 1995), but Van Straaten (1965) and Guillén and Hoekstra (1997) observed coarser material on the bar crests for the Dutch coast. Considerable spatial heterogeneity of the sediment grain size is also observed at rip-bar systems with coarser sediment in the rip-channels (MacMahan et al., 2005; Gallagher et al., 2011; Dong et al., 2015). Coarsening of the bed (change in median grain diameter D_{50} of about +150 µm) as a result of alongshore transport processes was observed at a large-scale sand nourishment at the Dutch coast ('The Sand Motor'; Huisman et al., 2016). This study also showed that the alongshore changes in D_{50} are related to spatial variability in the hydrodynamic forcing conditions.

The impact of storm conditions at natural coasts typically consists of a coarsening of the sediment grain size. Most prominent coarsening of the median grain diameter (D_{50} up to 100 µm coarser), during a storm event with offshore significant wave height of $H_{m0} = 4$ m, was observed in the swash zone (Stauble and Cialone, 1996). This coarsening gradually decreases in the offshore direction. Terwindt (1962) observed a quite uniform coarsening of ∼30 µm from 2 to 6 m water depth at the coast of Katwijk (The Netherlands) after a moderate summer storm (H_{m0} ≈2m). Numerical modelling of cross-shore transport sorting during storms also shows coarsening of the nearshore zone and subsequent fining of the offshore sediment at the toe of the deposition profile (Reniers et al., 2013; Sirks, 2013; Broekema et al., 2016). Seasonal variability of the cross-shore distribution of the grain size, as observed by Medina et al. (1994), comprised nearshore bed composition coarsening in winter ($H_{m0,winter}$ ≈4m) and restoration to a finer bed composition in summer ($H_{m0,summer}$ ≈1m). The largest annual variability in the measured D_{50} was observed in the swash zone (up to 200 µm) at mean sea level (MSL) which gradually decreased to a variability of ∼20 µm at MSL -8 m. Seasonal variability of the D_{50} was, however, found to be almost negligible for a nourishment at the Dutch barrier island of Terschelling (Guillén and Hoekstra, 1996). Guillén and Hoekstra (1996) observed an 'equilibrium distribution' of the size fractions, which means that the cross-shore bed composition of each size fraction will be restored over time by the hydrodynamic processes to the natural equilibrium situation. An influence of the width of the littoral zone (which depends on the wave conditions) on the location of transitions in the cross-shore grading of the sediment was suggested by Guillén and Hoekstra (1997).

Spatial variability of the grain size (on cross-shore profiles or alongshore) is often the result of differences in the behaviour of sediment grain size fractions for the same hydrodynamic forcing conditions (e.g. for bi-modal sand in Richmond and Sallenger, 1984). Sorting processes at the scale of the sediment grain can induce sorting mechanisms of which settling, entrainment and transport sorting are considered most relevant (Slingerland and Smith, 1986). Sorting due to settling, for example, plays a role in sedimentary environments where fine grains are deposited over a much larger distance than the coarse grains (Baba and Komar, 1981). Entrainment sorting

is the result of differences in the suspension of sediment grain particles into the water column, which is affected by the size and weight of the particle (Komar, 1987) as well as the density of the grains (Steidtmann, 1982). Investigations on the critical limit for suspension of the sediment into the water column were made by Bagnold (1966) (and other researchers) who indicates that the 'initiation of suspension' is related to the shear velocity at the bed ($u*$) and the fall velocity (w_s) of the sediment particle (see also Van Rijn, 1993). The finer sediment, that is suspended higher up in the water column (Rouse, 1950), is typically advected over a longer distance by the currents. The availability of the size fractions in the bed is also of relevance for the transport sorting as it determines the (reference) concentrations. These sorting processes may act together and induce a 'preferential transport' of (fine) sediment size fractions at locations where substantial gradients in the hydrodynamic forcing conditions are present. Hiding and exposure mechanisms (i.e. hiding of fine grains and exposure of coarse grains; Egiazaroff, 1965; Ashida and Michiue, 1973), on the other hand, may reduce the preferential transport for conditions which are at (or very close to) the critical shear stress for mobility of the sediment mixture. The individual sediment size fractions in the sand mixture (in unilateral flows) are then expected to behave similarly as they are mobilized at the same critical shear stress (Wilcock, 1993). Conditions in the marine environment are, however, typically above the mobility threshold and closer to the critical limit for initiation of suspension as a result of wave stirring (e.g. Holland coast; Huisman et al., 2016).

The modeling of changes in bed sediment composition can be performed either with data-driven models or numerical models. Data driven models use observed knowledge on the sediment distribution at the considered coast to derive the transport processes and/or predict future changes in bed composition. For example, Guillén and Hoekstra (1996) introduced the concept of an equilibrium cross-shore distribution of sediment size fractions for a beach at Terschelling (The Netherlands). Any change to the cross-shore distribution of a size fraction will result in a redistribution of sediment until the equilibrium cross-shore distribution is restored (Guillén and Hoekstra, 1996). McLaren and Bowles (1985) proposed a method to track the transport direction of (graded) sediment on the basis of spatial differences in the sediment grading. The derived properties of the grading (i.e. mean size, standard deviation and skewness) change in a logical way along the transport path. Other studies, however, suggest that only a better sorting provides a consistent proxy for the pathways of the sediment (Gao and Collins, 1992; Masselink, 1992).

Numerical models (e.g. Delft3D; Lesser et al., 2004) are more suitable than data-driven models for investigating situations where a local equilibrium is not available. Sediment transport rates and bed composition changes are computed per sediment size fraction on the basis of the forcing conditions in the numerical models (Van Rijn, 2007b). Typically an administration of bed composition changes is applied for a discrete number of layers of the bed and an active layer concept (Ashida and Michiue, 1973; Ribberink, 1987). The capability of numerical modelling of sediment transport with multiple size fractions was shown, for example, by Van Rijn (1997) for cross-shore sorting during storms. Furthermore, numerical modelling of sediment sorting was compared to field and laboratory experiments for a river bifurcation in the Netherlands (Sloff and Mosselman, 2012) and detailed sorting at river dunes (Blom and Parker, 2004). Even the generation of river deltas was modelled by Geleynse et al. (2011) who found that models could reproduce the typical plan-form shapes of river deltas which depends both on the supply of sediment and local hydrodynamics. Applications of numerical modelling of the redistribution of non-uniform sediment are, however, missing for sand nourishments at natural coast where a large influence of alongshore redistribution of sediment can be expected.

The objective of this work is to assess the relevance of hydrodynamic conditions for the development of heterogeneity in D_{50} just outside the surfzone of a large-scale nourishment. This required a validation of the numerical model Delft3D against observed spatial and temporal changes in D_{50} over a period of 2.5 years after construction of the large-scale 'Sand Motor' nourishment (Stive et al., 2013) to allow the investigation of underlying processes. Simplified hydrodynamic conditions were then used in the model to exemplify the influence of individual conditions.

2. Study Area

The study area is located between Monster and Kijkduin on the southern part of the Holland coast (the Netherlands). A large-scale sand nourishment referred to as the 'Sand Motor' was constructed here from April to June 2011 ($\sim$21.5 million m^3; Stive et al., 2013). The planform design of the Sand Motor comprised of a hook-shape with a dune lake and open lagoon on the landward side (Figure 1) with an alongshore extent of about 2.5 km and a cross-shore width of about 1 km at the waterline. The foot of the nourishment attaches to the natural bed at a depth of about 10 m.

Figure 1: Aerial photograph of the Sand Motor after completion (September 2011). Note the clouds of fine-grained material moving to the North. Picture courtesy of Rijkswaterstaat / Joop van Houdt

Bathymetric changes after construction of the Sand Motor were monitored at 1 to 3 month intervals. In the first period after completion a large morphological response of the Sand Motor was observed (de Schipper et al., 2016), as about 1.8 million m^3 of sand was spread alongshore. The initial blunt shape was reformed in a smooth planform shape (see Figure 2). The nearshore bathymetry at the Sand Motor is characterized either by sections with a longshore uniform bar-trough system or transverse bars (Rutten et al., 2017).

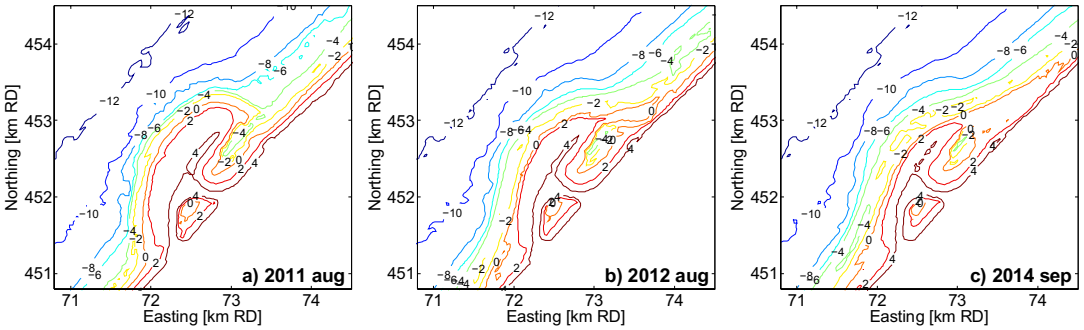

Figure 2: Sand Motor bathymetry directly after construction, after 1 year and after 3 year (bed level with respect to mean sea level).

The Holland coast wave climate is characterized by wind waves which originate either from the South-West (i.e. dominant wind direction) or the North-West (i.e. direction with largest fetch length). The average significant wave height (H_{m0}) is about 1 m in summer and 1.7 m in winter (Wijnberg, 2002) with typical winter storms with wave heights (H_{m0}) of 4 to 5 m and a wave period of about 10 seconds (Sembiring et al., 2015). The severest storms originate from the North-West and coincide with a storm surge of 0.5 to 2 m. Offshore wave data are available at an offshore platform ('Europlatform') at 32 m water depth. The horizontal tide is asymmetric with largest flow velocities towards the North during flood (~0.7 m/s) and a longer period with ebb-flow in southern direction (~0.5 m/s; Wijnberg, 2002). The tidal wave at this part of the North Sea is a progressive wave with largest flood velocities occurring just before high water. Tidal flow velocities at the Sand Motor are enhanced as a result of contraction of the flow (Radermacher et al., 2017). Mean bed shear stresses as a result of currents and waves (τ_{cw}) in the nearshore region of the Holland coast typically range from 0.1 to 10 N/m^2 (Huisman et al., 2016) which is an order of magnitude larger than the critical threshold for mobilization of the grains (τ_{crit} of about 0.04 N/m^2 for sand with a D_{50} of 300 µm). The shear stresses in deeper water may, however, be insufficient to fully suspend all sediment grain size fractions in the water column during normal conditions (i.e. less than 0.4 N/m^2 for 300 µm sand; Van Rijn, 1993).

Sediment sampling at the Sand Motor nourishment revealed large spatial heterogeneity of the D_{50} which developed after construction (Huisman et al., 2016). Sediment data at the Sand Motor were collected prior, during and (half)yearly after construction of the Sand Motor over a timeframe of 4 years (see Figure 3). Surfzone sediment samples were collected with a Van Veen grab and dry beach samples from land. The Van Veen grab sampler had a radius of about 15 cm and collects sediment from the top 5 to 10 cm of the bed. Typically, about 5 to 12 samples were taken for each transect between MSL-1m and MSL-10m and a few samples on the dry beach. A special survey with short-term (bi-weekly) changes of the bed composition was performed in October 2014.

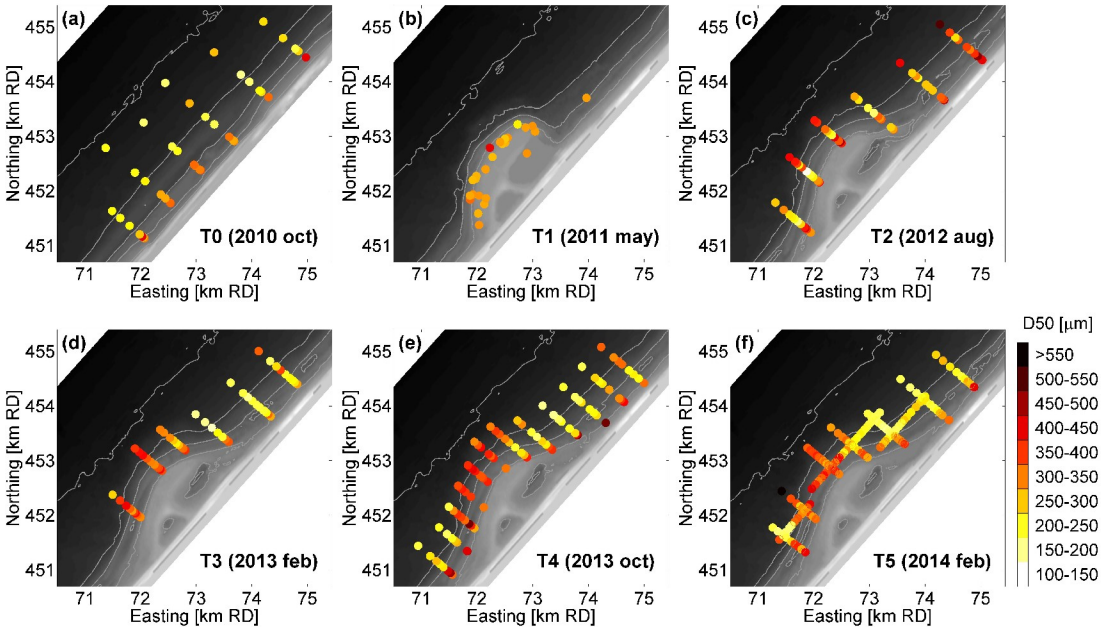

Figure 3: Median grain diameter of sediment samples for $T0$ to $T5$ surveys

As detailed in Huisman et al. (2016), the situation before construction of the Sand Motor (T0) was characterized by medium sand at the waterline (D_{50} of 300 to 400 µm) which gradually fines in seaward direction to a D_{50} of about 200 µm at MSL -7m and deeper (Van Straaten, 1965; see T0 situation in Figure 3). Dry beach and dune sediment generally consists of medium sand (200 to 300 µm; Kohsiek, 1984). Nourished sediment ($T1$) was relatively uniform and well mixed with an average D_{50} of 278 µm. The situation after construction of the Sand Motor (especially from the $T3$ survey and onwards) is characterized by significant coarsening of the bed sediment at the exposed part of the Sand Motor (~150 µm) and fining of the bed sediment just North and South of the Sand Motor (up to -50 µm; Figure 3). A narrower grain size distribution was observed at the Sand Motor with a standard deviation (SD) of 0.4 to 0.6 after construction while the reference situation and nourished sediment were moderately well sorted (i.e. SD ranging from ~0.6 to 0.8). A band with finer sediment was observed in the $T2$ survey between MSL -4m and MSL -8m, which aligns with observed cross-shore distributions of the D_{50} after a storm (Broekema et al., 2016). The $T2$ survey is, however, left out of consideration in this research as 1) the main focus is on long-term large-scale patterns of the D_{50} and 2) as there is uncertainty on the quality of the measured D_{50} in deeper water for this survey. The D_{50} in deeper water (far outside the region of influence of the Sand Motor) coarsened much more in the $T2$ survey (i.e. 50 to 200 µm coarser) than is expected based on understanding of the system, other field investigations or literature. Note that this research uses kilometer marks to describe cross-shore profile sections at the Center of the Sand Motor Peninsula (km 7), Northern flank (km 8) and North of the Sand Motor (km 9).

3. Methodology

The evolution of the bed composition at the Sand Motor was investigated with the aid of the numerical model Delft3D (Lesser et al., 2004). A 2.5 year hindcast of the bed sediment compo-

sition changes at the Sand Motor (with a focus on D_{50}) was made, which was validated against observed D_{50} from sediment sampling surveys at the Sand Motor (Huisman et al., 2016). The computed bed composition changes over the hindcast period were used to provide insight in the transport rates for each of the sediment size fractions and vertical grading of the bed. The relevance of the hydrodynamic forcing conditions (i.e. tide and waves) for the development of heterogeneity in the D_{50} was then further investigated in models with simplified hydrodynamic conditions.

Numerical model setup

The Delft3D model (Lesser et al., 2004) uses the shallow water equations for 2DH and 3D computations of the flow and a wave energy transport model (SWAN) for the wave transformation towards the shore (Booij et al., 1999). The curvi-linear grid covers the southern section of the Holland coast (9 km in alongshore direction and 4 km in cross-shore direction) with a resolution of about 34m x 17m near to the Sand Motor (Figure 4). The initial Sand Motor bathymetry, as measured directly after construction of the Sand Motor on 3 August 2011, was used as a starting point for the numerical models. Both 2DH and 3D modelling approaches were applied (with 12 vertical layers for the 3D model). Measurements from a wave bouy and two ADCP stations were available for validation of the modelled hydrodynamics.

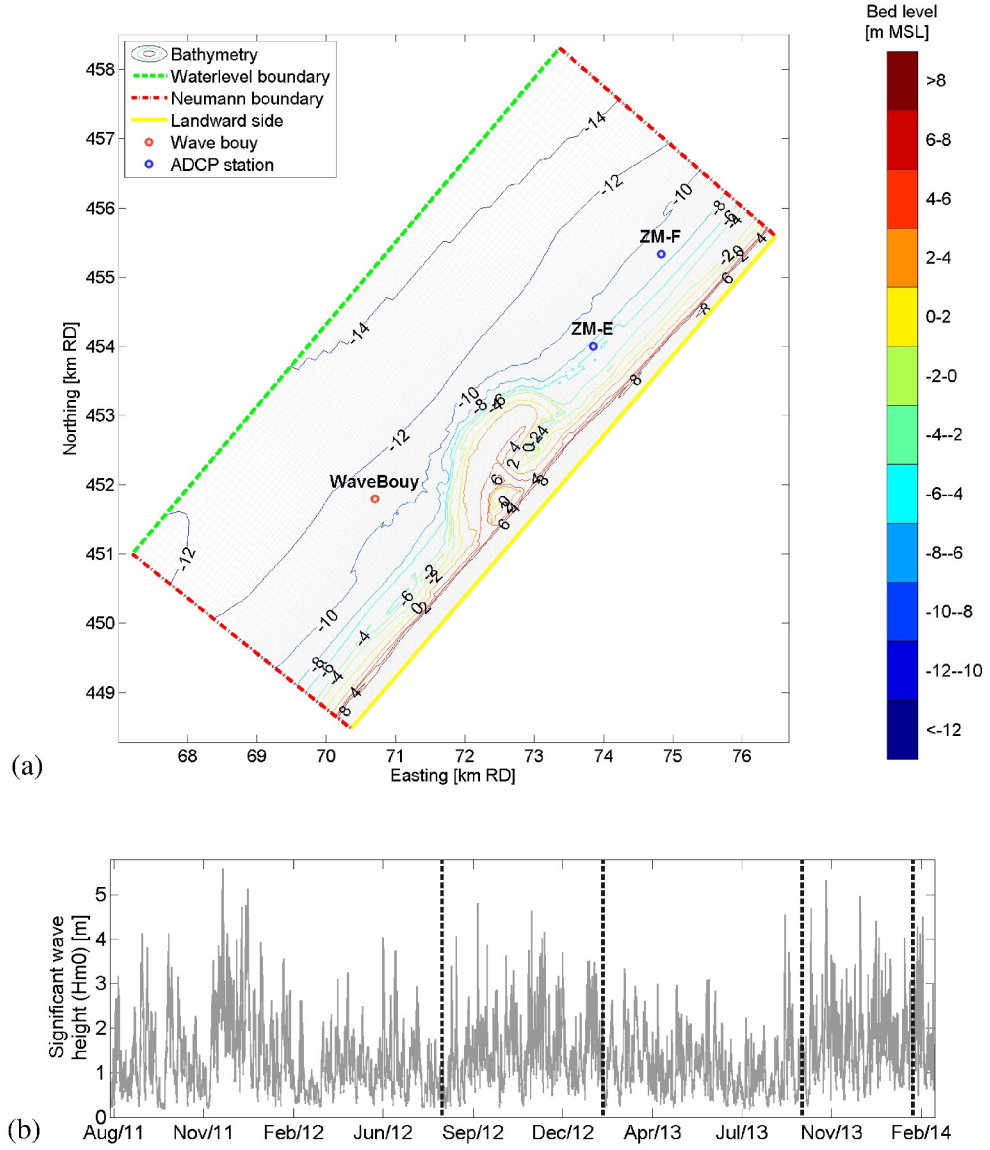

Figure 4: Model domain with initial bathymetry of August 2011 (a) and time-series of wave boundary conditions (b) from August 2011 to February 2014. Note that sediment sample surveys are shown as vertical dashed grey lines

Flow boundary conditions were derived from the CoSMoS model (Sembiring et al., 2015; Barnard et al., 2014) which provides continuous forecasts of the tidal currents and water levels in the North Sea. The water level boundary condition was applied at the seaward boundary of the model, while tidal currents were included as a water level gradient (i.e. Neumann type boundary) at the lateral boundaries. Offshore wave boundary conditions consisted of a full time-series of wave conditions at the 'Europlatform' measurement station from August 2011 to February 2014 (Figure 4). The roller model (Roelvink, 1993) was applied to distribute turbulence of the breaking waves over the surfzone.

Sediment transport was computed for predefined discrete size fractions (Van Rijn, 2007b) with the Transpor2004 formulation (Van Rijn et al., 2004; Van Rijn, 2007a). The reference concentrations of each of the size fractions are scaled according to their relative occurrence to make the transport rates of sediment with multiple size fractions comparable to uniform sediment (Van Rijn et al., 2004). The single fraction formulation performed well in the morphological hindcast of the first year development of the Sand Motor (Luijendijk et al., 2017).The morphological time scale in the model is four times the hydrodynamic time scale (Ranasinghe et al., 2011). The introduced discrepancy between the phase of the tide and the waves was found to have no significant influence on the long-term sorting pattern from a half-year test simulations with a morphological factor of one. Transport rates were calibrated (for all simulations) to 50% of the default uncalibrated value, which provided a good hindcast of the morphological changes at the Sand Motor for the model with a single sediment fraction (i.e. using the same settings as Luijendijk et al., 2017). This calibration parameter is within the typical expected range of the TRANSPOR2004 model as specified in the implementation manual (Van Rijn et al., 2004) and not much lower than the 0.6 which was (among other calibration factors) applied by Grunnet et al. (2005) for a morphological hindcast at Terschelling (The Netherlands). Additional to the overall calibration of the transport, also the transport due to wave skewness and asymmetry has to be adjusted in 2DH models in order to balance the cross-shore transport. The suspended transport due to waves ($SUSW$) of the 2DH model was set at 20% of the default value. The main reason for the strong reduction of this parameter is that the offshore-directed undertow (which normally balances out the onshore directed transport) cannot be represented in a 2DH model. This ratio of the $SUSW$ parameter is in line with literature suggesting a value of 0% to 50% for 2DH models (Van Rijn et al., 2004; Giardino et al., 2011). It is noted that the $SUSW$ calibration parameter hardly affects the alongshore transport rates.

A multi-layer approach with an active layer was used to administrate the bed composition changes (Ashida and Michiue, 1973; Ribberink, 1987; Sloff and Mosselman, 2012), which means that the contribution of each of the sediment size fractions is administrated per layer and per grid cell. A 'transport layer' is present at the top of the bed for which the bed composition is adjusted over time as a result of erosion and/or accretion of the modelled sediment size fractions (Figure 5).

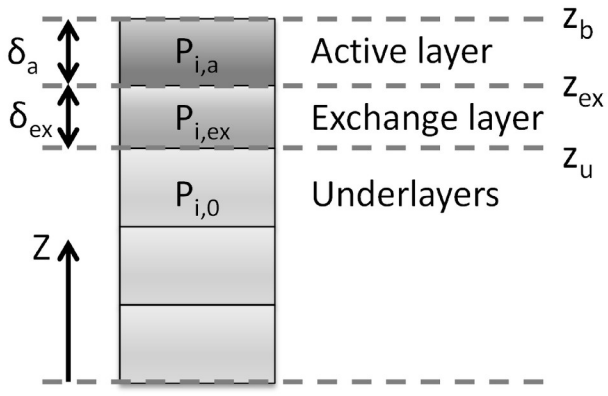

Figure 5: Multi-layer administration within Delft3D

The transport layer moves up and down with the bed when erosion or sedimentation takes place (i.e. with fixed thickness). During accretive situations the transport layer moves upward, which means that 1) newly accreted sediment is mixed proportionally with the existing material in the transport layer and 2) a representative part of the sediment of the transport layer is added to the layer underneath the transport layer (referred to as the 'exchange layer'). Analogously, sediment from the exchange layer is moved back to the transport layer when erosion takes place. The exchange layer has a variable thickness since its upper interface moves with the active layer, while layers below the exchange layer (referred to as 'underlayers') are vertically fixed. The vertical fixation of the underlayers prevents numerical diffusion of sediment into the substrate as a result of (temporary) changes in the morphology of the bed. A description of the mass balance for each sediment size fraction (Sloff and Mosselman, 2012) reads as follows:

$$\rho_s(1-\epsilon)\left(\frac{\partial(p_{i,a}\delta_a)}{\partial t}+p_i(z_0)\frac{\partial z_0}{\partial t}\right)+\frac{\partial q_{sxi}}{\partial x}+\frac{\partial q_{syi}}{\partial y}=0 \tag{1}$$

in which the level of the substrate below the considered layer is denoted as z_0 and the thickness of the layer as δ_a. The top level of the considered layer is $z_0+\delta_a$. The proportion of sediment of size fraction i at a layer is denoted as p_i which is taken equal to the proportion in the active layer ($p_{i,a}$) when sedimentation occurs and equal to the proportion of the layer below the considered layer ($p_i(z0)$) during erosion. q_{sxi} and q_{syi} are mass sediment transport components per unit width for fraction i in the x and y direction, which is per definition zero for the exchange layer and underlayers. ρ_s is the density of the sediment and t is time.

A thickness of the active layer of 0.1 m was applied in the models, as this is considered the zone which is mixed by the waves (see also Sloff et al., 2001). It is noted, that the actual thickness of the top layer has an effect on the rate of initial D_{50} changes, but had only a small impact on overall D_{50} after a few years. Twenty underlayers with a thickness of 0.5 m were used in the models to represent the substrate material.

Model run configurations

Hindcast models were set up for the period from August 2011 to February 2014 to assess the performance of a Delft3D model in hindcasting bed sediment composition changes at the Sand Motor. The hindcast models differ with respect to the number of vertical layers in the water column (2DH or 3D) and initial bed composition (Table 1), while the same grid was used for each of the models (34m x 17m). Furthermore, a reference simulation was made with only 1 sediment fraction of 278 µm sand ($H0$).

Table 1: Overview of the run configurations of the Sand Motor model hindcasts H0 to H3

Run	**Vertical layers**	**Bathy-metry**[*1]	**Transp. formula**	**Nr. frac.**	**Initial bed**	**Tide & Waves**
$H0$	2DH	ZM2011	Tr2004	1	uniform	Time-series (Aug 2011-Feb 2014)
$H1$	2DH	ZM2011	Tr2004	5	uniform	Time-series (Aug 2011-Feb 2014)
$H2$	3D (12)	ZM2011	Tr2004	5	uniform	Time-series (Aug 2011-Feb 2014)
$H3$	3D (12)	ZM2011	Tr2004	5	inibed	Time-series (Aug 2011-Feb 2014)

[*1] ZM2011 refers to the Sand Motor bathymetry of August 2011.

The models with a 'uniform' initial bed composition for the whole domain applied a D_{50} of 278 µm (similar to the Sand Motor sand). The grain size distribution at the Sand Motor was classified

in five size fractions according to Van der Zwaag (2014) (Table 2). The spatially varying initial bed composition ('inibed') consisted of the aforementioned sand mixture at the Sand Motor (i.e. D_{50} of 278 µm) and a natural fining of the sediment in the offshore direction at the adjacent coast (Figure 6). The applied 10th and 90th weight percentile diameter of the sand were respectively a factor 2.2x smaller or larger than the D_{50} which was similar to the ratio of the observed transect averaged D_{50}, D_{10} and D_{90}. The sediment at the Sand Motor was specified as separate sediment fractions from those at the adjacent coast, with the aim of discerning the behaviour of the Sand Motor sand from that of the rest of the coast.

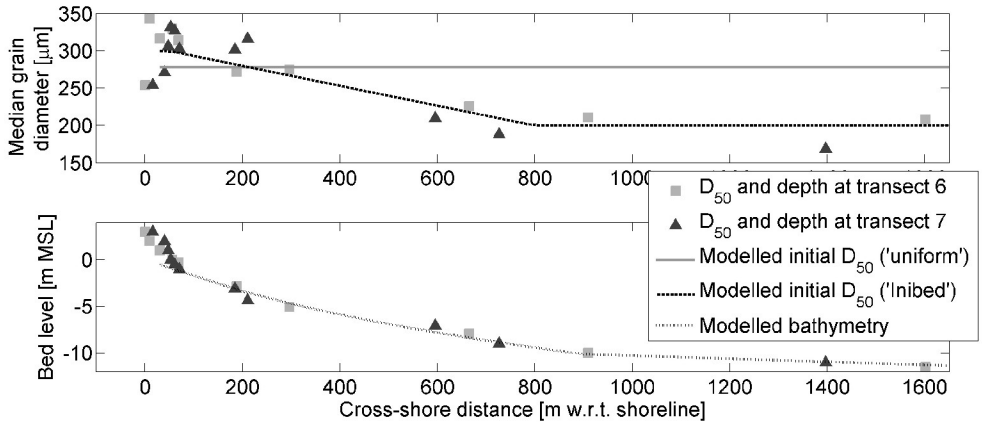

Figure 6: Cross-shore distribution of the measured D_{50} at the Sand Motor (T0 survey) and modelled initial bed

Table 2: Classification of the sediment distribution at the Sand Motor into five sediment size fractions

Class	**Lower limit [µm]**	**Median [µm]**	**Upper limit [µm]**	**Mass percentage**
1	63	107	150	9.5%
2	150	181	225	23%
3	225	256	300	24%
4	300	363	425	29%
5	425	513	1180	15%

The findings in the 3D model hindcast ($H2$), which was envisaged to provide a good representation of alongshore and cross-shore transport processes, were substantiated more with model configurations with simplified hydrodynamics (i.e. adjusted tide or waves), which aimed at isolating the relative importance of hydrodynamic forcing conditions (i.e. tide, normal waves and storm conditions) on the development of spatial heterogeneity in the D_{50}. Besides an average climate condition with H_{m0} of 1 m from 310 $^{\circ}N$ ($W1$) also variations of climate conditions were made with a different wave height (H_{m0} of 3 m wave height, $W2$) or with a sequence of a storm condition (H_{m0} of 3 m) after a moderate condition (H_{m0} of 1 m; $W3$). Also the sensitivity of the D_{50} changes for the wave direction ($\pm$ 30°) was evaluated ($W4$ and $W5$). Tidal conditions were investigated by simulating a situation without tide ($C1$), with only the tide ($C2$) or with a reduced or enhanced tidal velocity (at 80% or 120% of the actual tide; $C3$ and $C4$). Additionally, also the influence of a smaller seaward protrusion (of 200 or 400 m) of the nourishment bathymetry was modelled ($B1$ and $B2$). It is noted that the storm conditions (H_{m0} of 3 m) were

presented after 4 days, which is a realistic persistence for a year with relatively severe conditions along the Dutch coast.

Methods for quantifying model performance

The actual performance of the hindcast models was quantified on the basis of an inter-comparison of the modelled and observed D_{50} (Huisman et al., 2016). Both the representation of the alongshore heterogeneity of the D_{50} and the cross-shore distribution of the D_{50} was evaluated. A weighted average of the median grain size per cross-shore transect ($D_{50\mathrm{TR}}$) was computed, both for the field surveys and the models, with the aim of comparing the alongshore heterogeneity of the D_{50}. This $D_{50\mathrm{TR}}$ is defined as :

$$D_{50\mathrm{TR}} = \frac{1}{L}\sum_{i=1}^{n} D_{50,i}\Delta x_i \tag{2}$$

The contribution of each sample (landward of the MSL -10m contour) was computed by multiplying the median grain size of the sample ($D_{50,i}$) with the representative cross-shore extent (Δx_i, i.e. half of distance to neighboring sample). The summed D_{50} contribution of each sample was divided by the length of the considered transect (L). The agreement of the actual modelled and observed $D_{50\mathrm{TR}}$ was quantified by means of the squared correlation coefficient (R^2). Uncertainty in $D_{50\mathrm{TR}}$ as a result of the sampling methodology was estimated at $\sim$ 11 µm (Huisman et al., 2016), while uncertainty in D_{50} of individual samples estimated at 30 µm. Short-term temporal variability for moderate and storm conditions even amounts to a possible 40 to 80 µm difference for individual samples.

4. Hindcast of morphology and bed composition

Hydrodynamics and Morphology

Modelled currents and waves for the 2011-2012 winter period matched well with observations at local ADCP stations and a wave buoy (see Appendix A and Luijendijk et al., 2017). The patterns of erosion and sedimentation over the first two years after construction of the Sand Motor (from August 2011 till August 2013) were very similar, showing net erosion at the peninsula of the Sand Motor and accretion at the adjacent coast (Figure 7).

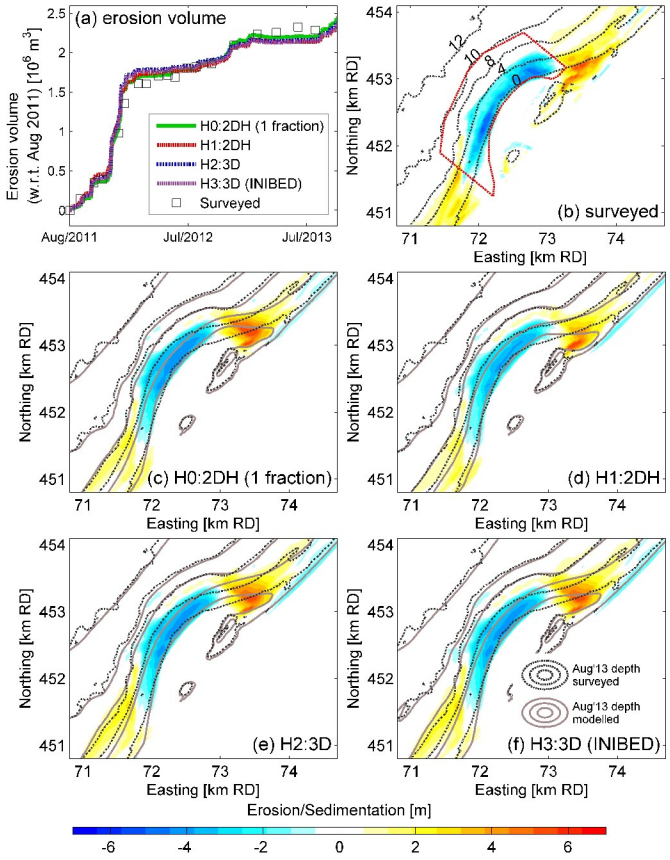

Figure 7: Bathymetric changes in the first two years after construction of the Sand Motor. Panel a shows the volume of erosion at the peninsula (i.e. within red dashed line in panel b), while panels b to f respectively show the surveyed and modelled bathymetric changes (from Aug 2011 to Aug 2013). Note that the MSL to MSL -12m contours for the surveyed and modelled bathymetries of August 2013 are presented respectively as dashed and continuous lines.

The erosion rates in a control area of $\sim$2 km^2 at the Sand Motor peninsula (Figure 7b) were almost identical to the observed changes (see erosion volumes in Figure 7a). The modelled erosion volumes also aligned well with the observed erosion of about 1.8 million m^3 by de Schipper et al. (2016) in the first year after construction of the Sand Motor. Models with multiple sediment fractions provided similar erosion rates as the model with a single sediment fraction (D_{50} of 278 µm). Reference is made to Luijendijk et al. (2017) for more detailed information on the morphological model performance of a single sediment fraction model.

The erosion and sedimentation patterns in the models (over the first two years) were also well represented in the models (Figure 7b to Figure 7f). The alongshore length of the region with erosion was very similar in the models and the survey, while the cross-shore distribution of the erosion was somewhat more gradual in the models. The most noticeable deviation concerned a seaward shift (of about 150 m) in the modelled location of the coastline on the northern flank of the Sand Motor (Figure 7), which can be seen from the difference between the modelled and surveyed depth contours (i.e. continuous and dashed grey lines). This dissimilarity between

the model and observed changes was slightly smaller in the simulations with multiple sediment fractions (compare panel c with panels d to f in Figure 7). An important notion from the sedimentation-erosion graphs is that most morphological change takes place in the nearshore (landward of MSL -6m), while field observations of bed composition at the Sand Motor have shown largest D_{50} changes outside the surfzone (i.e. from MSL -6m in seaward direction; Huisman et al., 2016). Subsequently, the region of interest for studying the D_{50} changes is not the same as the region where most morphological change takes place.
Overall, the morphological performance of the models is considered adequate for an investigation of the redistribution of the sediment size fractions at the Sand Motor which is expected to depend on the large-scale bathymetric and hydrodynamic characteristics of the Sand Motor (e.g. cross-shore extent, wave transformation and tidal contraction).

Transport rates

Computed two-year averaged transport rates at the Sand Motor (Figure 8) showed positive transport gradients at the Sand Motor (i.e. erosive) and negative at the adjacent coast (deposition), which induced a transport away from the Sand Motor. The transport rates of the single and multi-fraction models were similar in the nearshore region (from waterline to MSL-6m; compare $H0$ and $H1$ in Figure 8), which is in line with the observed similarities in the computed morphological changes. However, the transport rates in deeper water were enhanced considerably in the multi-fraction models ($H1$ to $H3$) as a result of the much larger mobility of the fine sediment size fractions compared to the average sediment grain size in the single-fraction model ($H0$). This holds especially for the 2DH model and to a lesser extent for the 3D model. The 3D model computes smaller sediment concentrations higher up in the profile (using the advection-diffusion equation) where the tidal currents act, while the depth-averaged current velocities in the 2DH and 3D models are very similar. Additionally, overall transport rates were enhanced in the model with the initial spatially varying bed composition ($H3$) which had more fine sand available in the bed.

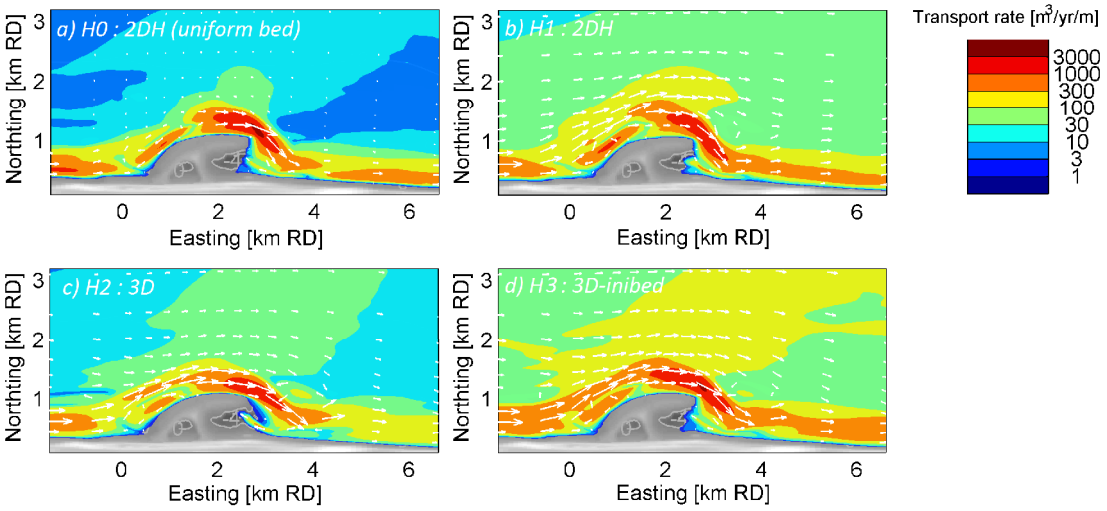

Figure 8: Time-averaged total transport for different model approaches of runs $H0$ to $H3$ (i.e. 2DH or 3D, single or multi-fraction approach and initially uniform or spatial varying bed composition). Note that transport is plotted with a logarithmic scale to visualize also the areas with moderate or low transport rates.

Bed composition changes (D_{50})

The computed bed composition (D_{50}) in the numerical models ($H1$ to $H3$ in Table 1) changed from a rather uniform initial D_{50} to a situation with considerable spatial heterogeneity in the D_{50} over a period of about 2.5 years (see time evolution of D_{50} in Figure 9). The models show the development of a typical spatial pattern in the D_{50} which is also observed in the measurements surveys ($T2$ to $T5$). This consisted of (1) an area with coarser sediment in front of the Sand Motor peninsula (from MSL -4 m to MSL -10 m), (2) a finer sediment composition just North and South of the Sand Motor and (3) a cross-shore variation in the sediment size with coarse sediment in the breaker zone and a fining of the sediment in the offshore direction. Computed 10th and 90th percentile grain size diameter (D_{10} and D_{90}) showed similar patterns as the D_{50}.

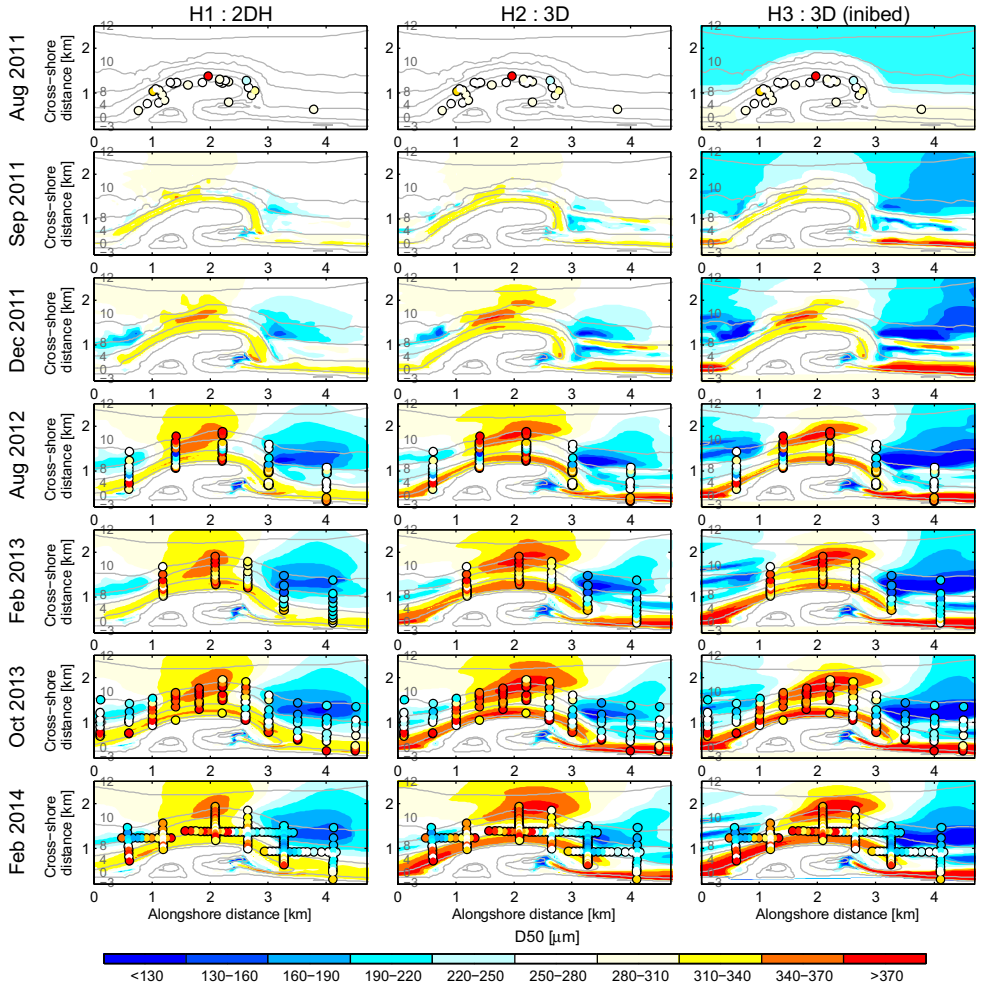

Figure 9: Development of spatial heterogeneity of the D_{50} over the first 2.5 years after construction of the Sand Motor for the 2DH, 3D and 3D-inibed models ($H1$, $H2$ and $H3$). Sediment survey data are shown as coloured markers. Depth contours are shown as continuous grey lines as a bed level in m MSL.

Qualitatively the 3D models (i.e. $H2$ and $H3$) provided the best agreement with the D_{50} patterns of the considered surveys (Figure 9), which represented both the magnitude of the coarsening of

the D_{50} in front of the Sand Motor peninsula as well as the fining on the northern side of the Sand Motor. The model with 2DH hydrodynamics ($H1$ in Figure 9) showed a less pronounced coarsening in front of the Sand Motor peninsula (MSL -4 m to MSL -12 m) than observed in the surveys (see February and October 2013). The initial bed composition was relevant for bed composition changes in deeper water (i.e. seaward of MSL -12 m at the Sand Motor and seaward of MSL -8 m at the adjacent coast).

The D_{50} patterns of the considered 3D models were very similar, irrespective of the initial condition that was used for the D_{50} of the bed (compare runs $H2$ and $H3$ in Figure 9). Consequently, the D_{50} patterns are considered to be the result of the hydrodynamic forcing conditions which acted on the models over the 2.5 year modelling period and subsequent morphological changes rather than the initial bed condition. Differences between the modelled and observed D_{50} patterns consisted of a relatively wide nearshore region with a coarse bed composition (D_{50} of 350 to 400 µm) and a smaller proportion of finer sand (200 to 250 µm) at ∼4 water depth at the northern side of the Sand Motor peninsula compared to the October 2013 and February 2014 surveys (Figure 9). This discrepancy is, however, expected to be related to the more seaward position of the modelled coastline on the northern flank of the Sand Motor compared to the observations (Figure 7) which results in a too seaward position of the surfzone with coarser D_{50}. A cross-shore shift of the modelled D_{50} of the bed was therefore used for transects at the northern flank of the Sand Motor in order to obtain an evaluation of the modelled alongshore and cross-shore bed sediment composition changes rather than the morphological performance. For this purpose the difference in depth of the modelled and observed bathymetry was minimized (i.e. the average distance between depth contours from MSL to MSL -10m).

A comparison of modelled transect averaged median grain diameters ($D_{50\mathrm{TR}}$) against observations showed that the aggregated model predictions were in good agreement with the data (comparison of $D_{50\mathrm{TR}}$ for October 2013 survey in Figure 10a). The 2DH model ($H1$) reproduced a very similar trend of the $D_{50\mathrm{TR}}$ with small scatter (i.e. highest R^2; Figure 10b), which suggests that 2DH processes provide a large contribution to the development of the alongshore D_{50} heterogeneity which is in line with Huisman et al. (2016). The $D_{50\mathrm{TR}}$ at the flanks of the Sand Motor deviated more for the 3D models ($H2$ and $H3$) as a result of the mentioned cross-shore shift in the morphology. The absolute $D_{50\mathrm{TR}}$ (i.e. 1 on 1 line in the scatter plots) was, however, better represented in the 3D models ($H2$ and $H3$), which is shown from a closer resemblance of the 1 on 1 line of the average modelled and observed $D_{50\mathrm{TR}}$ (Figure 10c and Figure 10d).

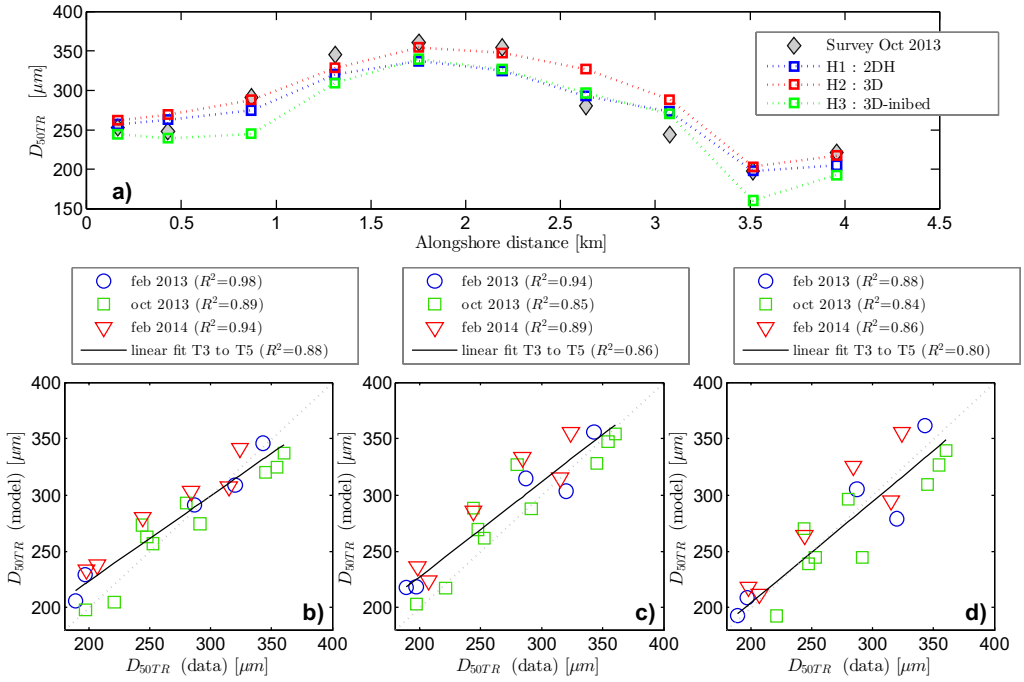

Figure 10: Measured and modelled transect averaged median grain diameter ($D_{50\mathrm{TR}}$) of the hindcast models $H1$ to $H3$ for surveys $T3$ to $T5$. (a) Alongshore variation of $D_{50\mathrm{TR}}$ for October 2013 survey; (b) Scatter plot of measured and observed $D_{50\mathrm{TR}}$ for $H1$: 2DH model, (c) $H2$: 3D model and (d) $H3$: 3D-inibed model.

The cross-shore variation of the D_{50} at three representative cross-shore transects (at the Peninsula, northern flank and North of the Sand Motor) was well represented in the models (i.e. R^2 of 0.4 to 0.9; Figure 11). Especially the 3D models resolved the details of the cross-shore distribution of the sediment, such as the small depression in D_{50} (at x=300 m) at the Sand Motor Peninsula in the February 2013 survey and the small increase in D_{50} North of the Sand Motor in the October 2013 survey. The 2DH models provided a more smoothed cross-shore distribution of the D_{50}. It is noted that a compensation was made for the bathymetric shift (of about 150 m) for the transect at the Northern flank of the Sand Motor, while transects at the Sand Motor Peninsula and North of the Sand Motor were shifted only marginally (i.e. typically ∼40 m). Similar performance was observed for the February 2014 survey (with R^2 ranging from 0.4 to 0.9) and the August 2012 survey (R^2 of 0.3 to 0.6).

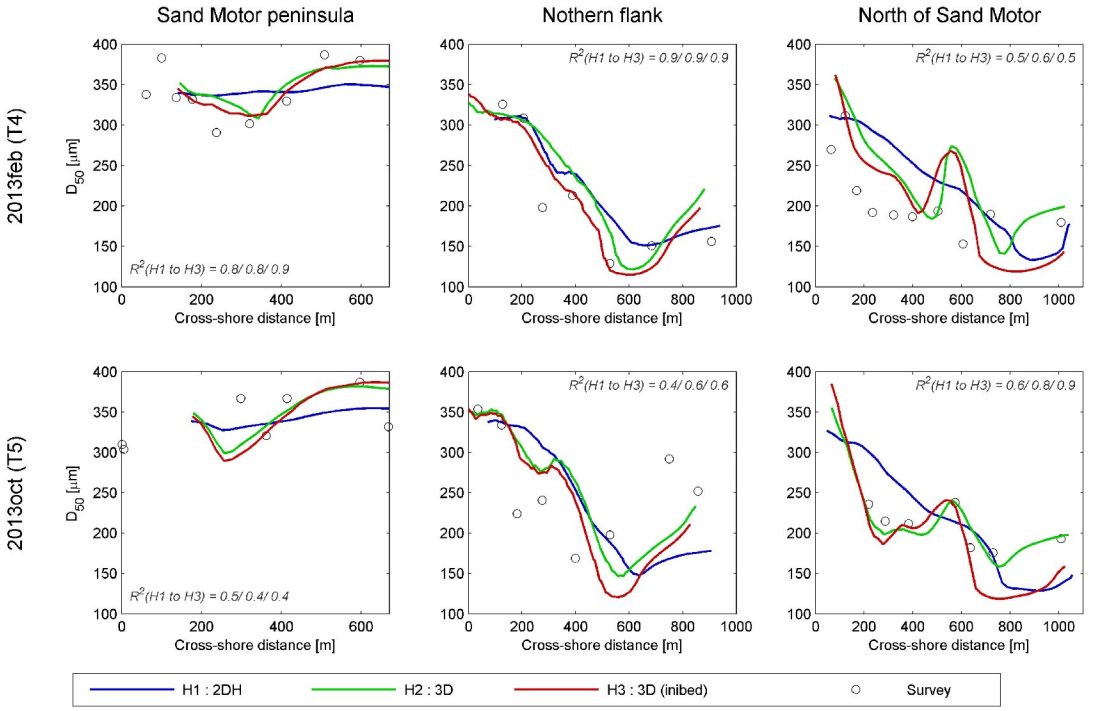

Figure 11: Median grain diameter on cross-shore transects at the center of the Sand Motor peninsula (tr=7), northern flank (tr=8) and North of the Sand Motor (tr=9) for $T3$ and $T4$ surveys. Performance expressed as R^2 is presented for $H1$, $H2$ and $H3$ respectively with grey text in the figure panels.

In summary, a 3D model is considered essential to represent both the alongshore and cross-shore patterns of the D_{50} at a large-scale nourishment and surrounding coast, while 2DH models can still reasonably represent the large-scale pattern of the D_{50} and the changes in the D_{50} of the bed in the alongshore direction. Additionally, an accurate initial (spatial varying) bed composition can be relevant for a precise representation of the magnitude of the $D_{50\mathrm{TR}}$ changes, but is not essential for the D_{50} in the nearshore (i.e. landward of MSL -8m).

Vertical grading of the bed

A closer look at the modelled D_{50} at the Sand Motor reveals that bed composition changes predominantly take place in the top-layer of the bed (Figure 12; $H2$ model). This is especially the case at the central Sand Motor transect, where erosion induced a coarsening of the top-layer material which extents well beyond the initial perimeter of the Sand Motor (Figure 12a). Furthermore, a thin layer of fine sand is present in deeper water just North and South of the Sand Motor (seaward of MSL-10m). On the other hand, a layer of up to a few meters of sediment accumulated at the landward side of the cross-shore profile (Figure 12, panel b and c). The coarser fractions accumulated in the nearshore region ($D_{50} \sim 350$ µm) at the flanks of the Sand Motor while the finer sediment size fractions are transported to deeper water (100 to 200 µm sand at MSL -10m) and further away in alongshore direction from the Sand Motor peninsula. Furthermore, a sequence of upward coarsening developed at the spit of the Sand Motor (see panel b of Figure 12 at x=3500 m). Finer sand fractions were deposited here initially, while over time the finer sand was covered by coarser sediment size fractions when the morphological footprint of the Sand Motor became wider. A very similar grading of the bed was found for the

$H3$ model, but then super-imposed on the initial bed composition that was provided to the model.

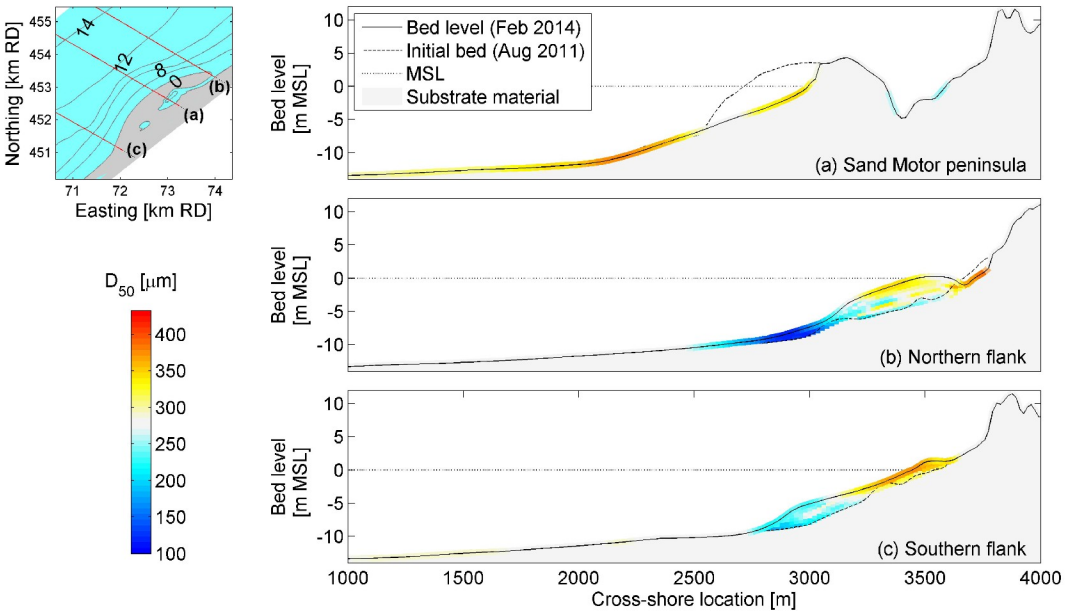

Figure 12: Vertical grading of the D_{50} of the bed at three cross-shore transects at the center of the Sand Motor and in the accumlation zones North and South of the Sand Motor (3D model : $H2$, February 2014).

The origin and destination of the Sand Motor sediment (which was marked as a separate fraction) was tracked for each of the size fractions, which shows that the fine sediment size fractions are redistributed over a much larger area than the coarse size fractions (Figure 13). The finest sediment fraction (63 to 150 µm) was transported both inside and outside the surfzone (up to MSL-12m on the northern side of the Sand Motor), while the medium and coarse fractions are transported almost exclusively in the nearshore (about 800 m wide section on the northern and southern side of the Sand Motor). The fine-medium sand fraction (150 to 225 µm) had in-between behaviour and was still distributed partially by the tide. It is noted that the computed cross-shore width of the zone with transport of finer sediment size fractions is also in line with visual observations of fine sand plumes being expelled from the Sand Motor (Figure 1). The observed fining of the bed in deeper water North of the Sand Motor (Figure 12) is therefore expected to be also the result of the abundance of alongshore supply of the finer sand fractions (63 to 225 µm) from the Sand Motor body.

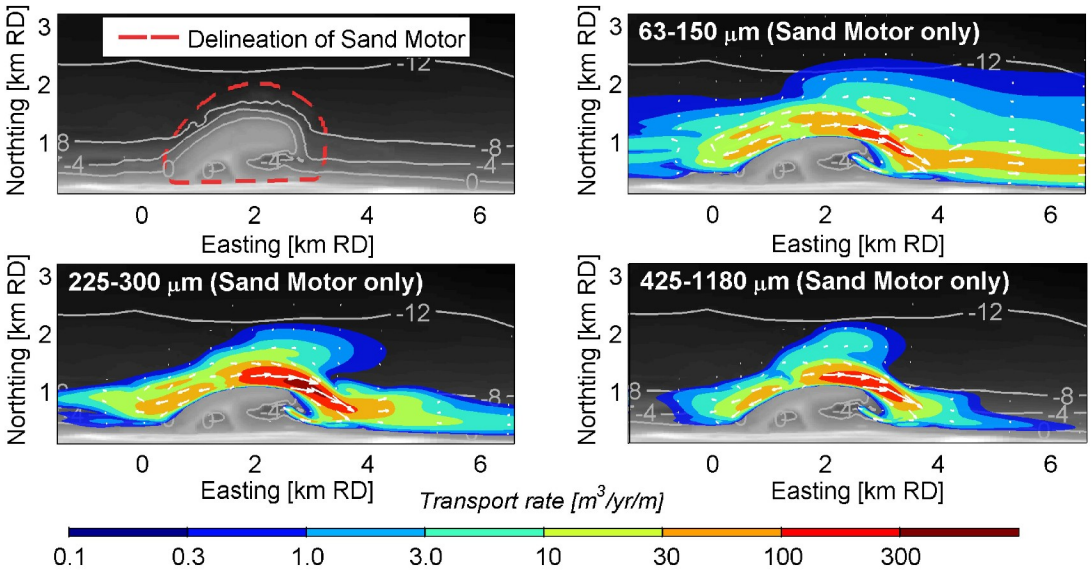

Figure 13: Time-averaged total transport for three sediment size fractions ($H2$: 3D model). Note that the transport is plotted with a logarithmic scale to visualize also the areas with moderate or low transport rates.

5. Relevance of hydrodynamic conditions

Model simulations with simplified hydrodynamics at the Sand Motor were used to identify the relevance of tide and waves for the generation of the coarsening at the Sand Motor and deposition regions at the adjacent coast. Simulations of storm and normal conditions (Figure 14a and Figure 14b) showed that coarsening of the D_{50} in front of the Sand Motor developed especially during normal wave conditions (run $W1$), while a less extensive coarsening of the bed developed as a result of the storm wave conditions (run $W2$). It is noted that the duration of the conditions was scaled down to a realistic duration (respectively 64 and 4 days for the normal and storm wave condition). The precise duration of the simulations was, however, not of influence to the general finding that the storms contribute far less to the coarsening at the Sand Motor, because the size of the coarse patch was still relatively small after a storm condition of a month (i.e. run $W2$ compared to run $W1$). This is also shown by a simulation of a storm condition after a period with normal conditions (run $W3$) which resulted in a small fining of the bed seaward of MSL -8m. The storm conditions, on the other hand, had a clear impact on the deposition regions North and South of the Sand Motor. The magnitude of the fining and area of this region was considerably larger for situations with storm conditions, which is related to the larger supply of sediment that is eroded from the coast.

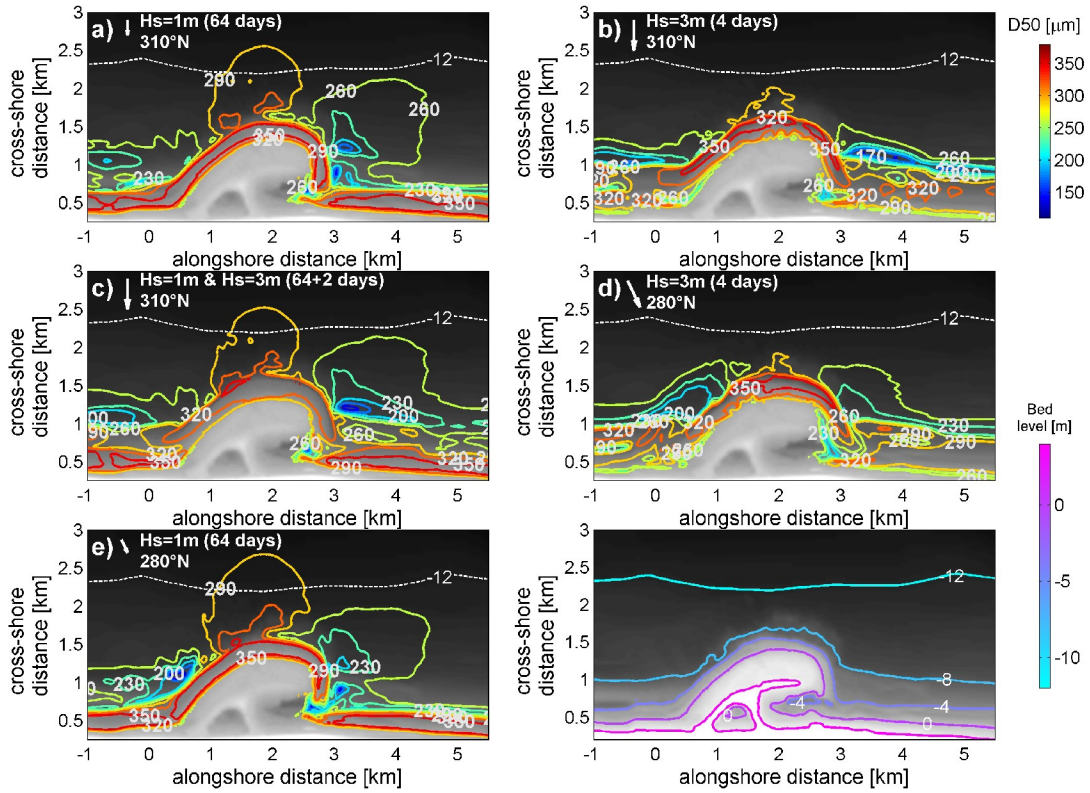

Figure 14: Modelled spatial pattern of D_{50} as a result of normal or storm conditions for shore-normal and oblique wave incidence using tide at Sand Motor (i.e. same tide signal as hindcast). a) Run $W1$ with H_{m0}=1m; b) Run $W2$ with H_{m0}=3m, dur=4 days; c) Run $W3$ with H_{m0}=3m, dur=2 days after 64 days with H_{m0}=1m; d) Run $W5$ with H_{m0}=3m, dur=4 days from 280°N; e) Run $W4$ with H_{m0}=1m from 280°N.

The direction of the incoming waves had only a small influence on the coarsening of the bed in front of the Sand Motor peninsula with slightly more coarsening for waves from the South-West (W4; Figure 14f). Wave direction did, however, affect the extent and magnitude of the deposition at the flanks of the Sand Motor during storm conditions (W5; Figure 14e), although the magnitude of the storm waves was still dominant.

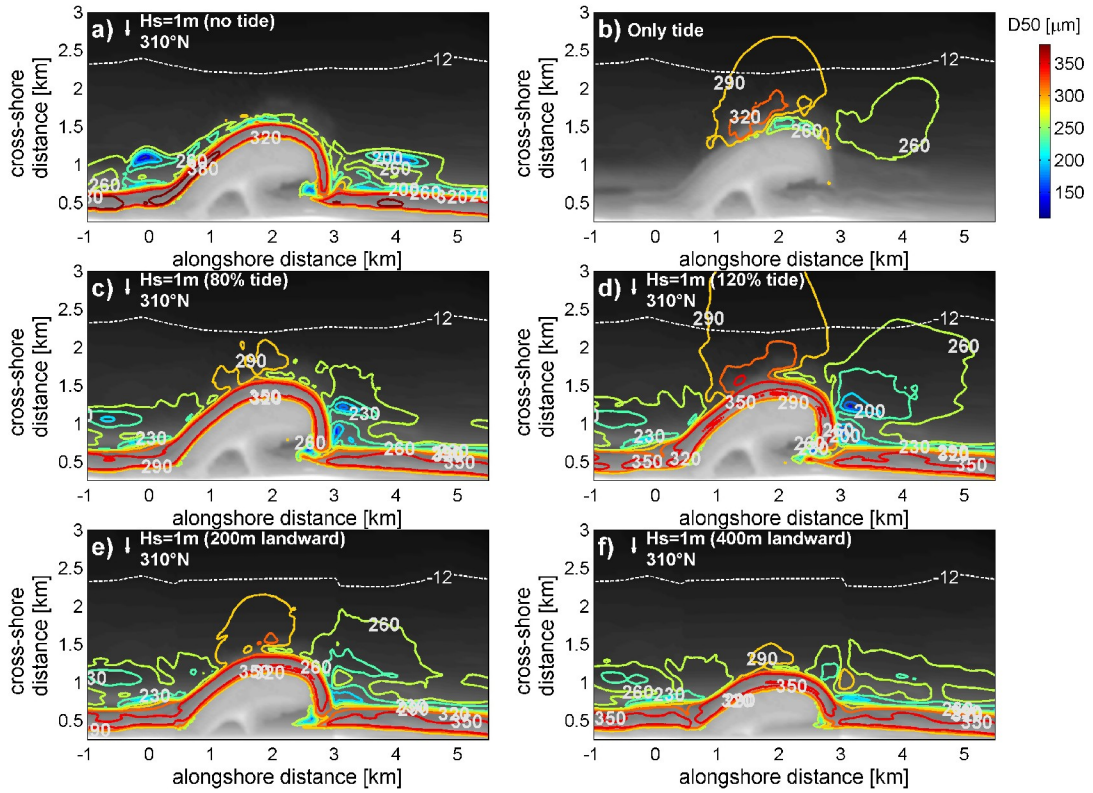

Figure 15: Modelled spatial pattern of D_{50} as a result of wave conditions (H_{m0}=1m), tide (ΔH ≈1.5m and $\hat{U}$ ≈1m/s) or adjustments of the bathymetry (affecting the tide and waves). a) Run $C1$ with only waves; b) Run $C2$ with only tide; c) Run $C3$ with 80% tidal velocities and moderate waves (H_{m0}=1m); d) Run $C4$ with 120% tidal velocities and moderate waves (H_{m0}=1m); e) Run $B1$ with 400 m landward shift of bathymetry (H_{m0}=1m and 100% tide); f) Run $B2$ with 200 m landward shift (H_{m0}=1m and 100% tide).

Simulations with either only waves or tide (run $C1$ and run $C2$) indicated that waves induce both a coarsening of the bed in the zone with the alongshore wave-driven current as well as patches with fine sand outside the surfzone on the flanks of the Sand Motor (Figure 15a), while tidal conditions were most relevant for the development of the coarsening of the bed outside the surfzone and induced a fining of the bed in deeper water at the adjacent coast (Figure 15b). The relevance of the tide is even further substantiated from simulations with enhanced and reduced tidal velocities ($C3$ and $C4$ in Figure 15c and Figure 15d) which show that the extent and magnitude of the coarse patch in front of the Sand Motor as well as the deposition region at the adjacent coast scale with the tidal velocities. The actual configuration of the Sand Motor also plays a role since spatial variation in D_{50} was hardly present for nourishment configurations with a (200 or 400 m) reduced cross-shore extent of the initial nourishment planform ($B1$ and $B2$ in Figure 15e and Figure 15f), which is related to a reduction of the contraction of the tide (i.e. less enhancement of tidal velocities) for these configurations.

In summary, a strong influence of the tidal velocities on the coarsening at the lower shoreface of the Sand Motor was found, which is the result of the enhanced forcing conditions due to the tidal contraction. It is expected that a preferential transport of fine sediment size fractions towards the adjacent coast is present which results in the coarsening of the top-layer of the bed (Huisman

et al., 2016). The much smaller coarsening of the D_{50} for the bathymetries with a reduced seaward protrusion of the nourishment also suggests that the tidal contraction is an important cause for the coarsening of the D_{50} of the bed. Storm wave conditions on the other hand were found to reduce the coarsening of the bed at the Sand Motor as a result of the mobilization (and supsension) of all of the sediment size fractions, because these conditions remove part of the relatively coarse top-layer. It is noted that deposited finer sand at the lower shoreface North and South of the Sand Motor did not necessarily only come from the coarsened region in front of the peninsula, but is occasionally also transported seaward from the nearshore zone during storm events with the undertow current. The extent of the deposition region at the flanks of the Sand Motor is therefore also determined by storm events.

6. Discussion

Our results show that the development of large-scale alongshore D_{50} heterogeneity at the Sand Motor can be reproduced well with the present numerical model. The observed pattern of coarsening of the D_{50} in front of the Sand Motor peninsula (in particular outside the surfzone) and fining at the adjacent coast were reproduced in models with different initial conditions for the D_{50} of the bed, which suggests that the hydrodynamic processes are responsible for the changes in bed composition (Figure 9). The transect averaged median grain size ($D_{50\mathrm{TR}}$; Figure 10) was modelled well with 2DH and 3D models (R^2 of 0.84 to 0.94), while the cross-shore distribution of the D_{50} and short-term variability during storms was reproduced best with a 3D modelling approach (Figure 11). The inclusion of the initial spatial varying bed composition provided a small improvement of the modelled alongshore heterogeneity of the D_{50} at the Sand Motor, but may be of large relevance if the applied nourishment sand is very different from the natural sediment or for situations where morphology is strongly influenced by the bed sediment condition (e.g. tidal estuaries or river bed dynamics; Dastgheib et al., 2008; Blom and Parker, 2004). The differences between the modelled and observed D_{50} patterns were small and mainly present on the flanks of the Sand Motor, which was also the location where morphology of the bed was somewhat less well predicted (i.e. too small erosion on northern flank of Sand Motor). These secondary discrepancies may relate to a variety of processes, of which their relative importance is not yet known, such as 1) seaward directed rip-currents of the nearshore bar-rip system (Gallagher et al., 2011), 2) alongshore directed currents from the sides to the center of the Sand Motor due to large-scale tidal eddies (Radermacher et al., 2017) and 3) secondary currents as a result of the fresh water plume of the Rhine (Visser et al., 1994) which can generate an onshore current near the bed in intermediate water depth (i.e. from the lower shoreface up to about 6 m water depth; Meirelles et al., 2017).

Large-scale coarsening of the D_{50} of the bed just outside the surfzone (i.e. seaward of MSL -6m) of large-scale nourishments (such as the 'Sand Motor') is mainly the result of the tidal currents (Figure 14). The local contraction of the tide results in a more frequent exceedence of the critical bed shear stresses for suspension of especially the finer sediment size fractions ($\tau_{crit,SUS}$; Van Rijn, 2007a) and subsequently also in a larger entrainment (Komar, 1987) and enhanced transport rate (Steidtmann, 1982) of these fine sand fractions. The difference in the suspension behaviour of the fine and coarse size fractions is expected to be largest during quiet and moderate wave conditions when the fine sand fraction is suspended while the coarse sand fraction is not, which is shown schematically in Figure 16 for a location on the lower shoreface of a large-scale nourishment (based on information on sediment concentrations from the Sand Motor model at 11 m water depth). A preferential transport of the finer sediment size fractions away from the Sand Motor is therefore present during normal conditions (Huisman et al., 2016), which removes

the fine sediment size fractions from the top-layer of the bed at the lower shoreface of the Sand Motor (Figure 12). It is noted that this process of coarsening by removal of the fine sediment fraction takes place even when the actual morphological changes are small. Over time the discrepancy in transport rates between the fine and coarse size fractions is expected to reduce, as concentrations of fine material in the bed will decrease. Eroded fine sediment from the lower shoreface of the Sand Motor is transported predominantly in northward direction to the adjacent coast (Figure 13; MSL -8m to MSL -12m), which is the result of the tidal asymmetry with larger north-going flood velocities, which explains the relatively large size of the fine sediment patch on the northern side of the Sand Motor (compared to the small fine sediment patch at the southern side). A nourishment with a smaller seaward protrusion (i.e. reduction of 25% or 50%) shows a less pronounced coarsening of the bed since the tidal contraction -which is considered the principal driver for the erosion of the bed- is reduced considerably. This suggests also that alongshore heterogeneity in D_{50} is likely to develop at other coastal structures which induce a contraction of the tide (e.g. port structures).

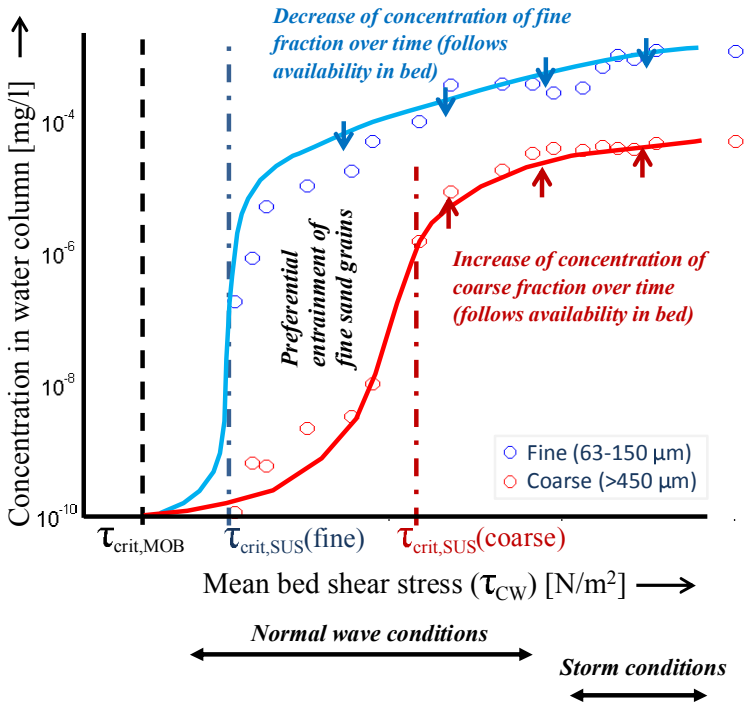

Figure 16: Schematic of the difference in suspension behaviour of fine and coarse sand fractions for moderate and storm conditions. The modelled time-averaged sediment concentrations at a location seaward of Sand Motor peninsula (E71856m, N453237m RD at 11 m water depth) of the 3D model ($H2$) are presented as circular markers for the coarse and fine sand fraction. Note that the typical range of bed shear stresses for normal and storm conditions is shown below the graph (see Huisman et al., 2016).

Extreme wave conditions reduce the magnitude and size of the coarse sediment patch at the lower shoreface of the Sand Motor (i.e. roughly from MSL -6m to MSL -12m), while waves would typically generate a coarsening of the D_{50} in the surfzone (Terwindt, 1962; Stauble and Cialone, 1996). Additionally, deposition of (relatively fine) sand from the nearshore region can take place at intermediate depths (i.e. between MSL -4m and -8m) during storm events (Reniers

et al., 2013; Broekema et al., 2016) which was also observed in the model, but cannot explain the reduction of the size of the coarse sediment patch at the lower shoreface (i.e. in deeper water). Instead, the fining of the D_{50} at the lower shoreface during a storm is considered the result of 1) the mobilization of all the size fractions (i.e. when both fine and coarse sand fractions are suspended in the water column; Figure 16) and 2) mixing of the coarse top-layer of the bed with relatively fine substrate sediment. Consequently, both the fine sand as well as the coarse top-layer are (partially) removed during a storm event. The small influence of the direction of the waves (Figure 14) on the coarse sediment patch is considered an indication that especially the stirring of the waves is of influence to the development of the coarse sediment patch. It is noted that such a relative fining of the D_{50} of the lower shoreface during was also observed during the storm of 22 October 2014 (Huisman et al., 2016).

The cross-shore extent of the region with transport of the finer sand fractions at a large-scale nourishment is much wider than the cross-shore footprint of the coarser sand fractions (Figure 13). This indicates that the medium and coarser sand fractions (>225 µm) are transported mainly by the wave-driven alongshore current, while the finer sand fractions (65 to 225 µm) are also mobilized by the tide. Consequently, the redistribution behaviour of the coarse and fine sand fractions is different. Especially the sediment redistribution in the zone outside the surfzone will be dominated by the behaviour of the finest sand fraction, which means that an approach with a uniform sediment grain size will underestimate the transport rates in deeper water. Theoretically, the alongshore transport of different size fractions (in deeper water) may even be bi-directional (e.g. if the tide velocities are very a-symmetrical or when waves approach from one side), similar to the observed bi-directional cross-shore transport of bi-modal sand at Duck (Richmond and Sallenger, 1984). Modelling of the morphological changes in deeper water therefore requires an approach with multiple sediment size fractions. The multi-fraction approach is essential for the evaluation of the environmental impact of a large-scale nourishment (or port construction). Models with uniform sediment can, however, still be applied well for situations where all of the sediment size fractions are mobilized, such as the assessment of the lifetime of sand nourishments for which the dominant processes take place in the nearshore region. Initial erosion volumes at the Sand Motor could, for example, be hindcasted well with both the single and multi-fraction models (Figure 7; Luijendijk et al., 2017).

7. Conclusions

The numerical model Delft3D was applied for a 2.5 year hindcast of bed sediment composition (D_{50}) at a large-scale sand nourishment ('Sand Motor'). Our findings indicate that the observed spatial pattern of the D_{50} at the Sand Motor (i.e. coarsening of the bed at the lower shoreface (i.e. outside the surfzone) in front of the peninsula and fining in deeper water just North and South of the Sand Motor) was reproduced well with the Delft3D model independent of the starting condition of the D_{50} of the bed. Both 2DH and 3D models reproduce alongshore variation in the D_{50} at such a large-scale nourishment (R^2 of 0.84 to 0.94) while cross-shore variation is represented only in a 3D model.

The development of the coarsening of the (top-layer of the) bed in front of a large-scale nourishment (or other coastal structure) is attributed mainly to the contraction of the tide. The locally enhanced current velocities result in a more frequent exceedence of the critical bed shear stress for suspension of the sediment, which induces enhanced entrainment of especially the fine sand fractions and subsequent preferential transport of the fine sand fraction to the adjacent

coast. Storm wave conditions, on the other hand, can induce a partial removal of the coarse top-layer of the bed on the lower shoreface (i.e. between MSL-6m and MSL-12m) in front of the large-scale nourishment. This is due to mobilization (and erosion) of both the coarse and fine sand fractions of the coarse top-layer and mixing with the relatively fine substrate sediment. Additionally, storm wave conditions induce a relative fining in deeper water at the flanks of the large-scale nourishment.

The finer sand fractions of a large-scale nourishment are distributed over a considerably larger (cross-shore) area than the coarser sand fractions. Typically, the coarse sand fractions are transported only in the surfzone by the wave-driven alongshore current while the fine sand travels also in deeper water with the tide. A modelling approach with multiple sediment size fractions is therefore required when the transport rates or morphological changes in deeper water are investigated. It is emphasized that this is of relevance for the assessment of the environmental impact (bed composition changes D_{50}) of any coastal measure with a large seaward protrusion (i.e. which creates contraction of the tide). An approach with a single sediment size fraction can, however, still provide a good performance for situations where all of the sediment size fractions are suspended into the water column. For example, when the erosion volume of a (nearshore) nourishment is investigated which is mainly determined by sediment transport in the nearshore zone.

Acknowledgments

The European Research Council of the European Union is acknowledged for the funding provided for this research by the ERC-advanced Grant 291206-NEMO.
This research is additionally supported through the NatureCoast project (no. 12686) by the Dutch Technology Foundation STW, which is part of the Netherlands Organisation for Scientific Research (NWO), and which is partly funded by the Ministry of Economic Affairs. This research is additionally supported by the Dutch Technology Foundation STW Grant 12686: Nature-driven Nourishments of Coastal Systems (NatureCoast). The STW foundation is part of the Netherlands Organisation for Scientific Research (NWO), which is partly funded by the Dutch Ministry of Economic Affairs. Sampling data for the years 2010, 2012 and October 2013 were collected with support of the European Fund for Regional Development (EFRO) which was taken care of by Jeroen Wijsman of IMARES and Pieter-Koen Tonnon of Deltares. Jelle van der Zwaag is acknowledged for exploring the potential for assessing sediment sorting within Delft3D models.

References

Ashida, K. and Michiue, M. (1973). Studies on bed load transport rate in alluvial streams. *Japan Societey of Civil Engineers*, 4.

Baba, J. and Komar, P. D. (1981). Measurements and analysis of settling velocities of natural quartz sand grains. *Journal of Sedimentary Petrology*, 51:631–640.

Bagnold, R. A. (1966). An approach to the sediment transport problem from general physics. *Geological Survey Professional Papers, Washington, USA*, 422-1:1–37.

Barnard, P. L., van Ormondt, M., Erikson, L. H., Eshleman, J., Hapke, C., Ruggiero, P., Adams, P. N., and Foxgrover, A. C. (2014). Development of the Coastal Storm Modeling System (CoSMoS) for predicting the impact of storms on high-energy, active-margin coasts. *Natural Hazards*, 74 (2):1095–1125.

Blom, A. and Parker, G. (2004). Vertical sorting and the morphodynamics of bed form-dominated rivers: A modeling framework. *Journal of Geophysical Research*, 109(F2):2156–2202.

Booij, N., Ris, R. C., and Holthuijsen, L. H. (1999). A third-generation wave model for coastal regions 1. Model description and validation. *Journal Of Geophysical Research*, C4, 104(C4):7649–7666.

Broekema, Y. B., Giardino, A., Van der Werf, J. J., Van Rooijen, A. A., Vousdoukas, M. I., and Van Prooijen, B. C. (2016). Observations and modelling of nearshore sediment sorting processes along a barred beach profile. *Coastal Engineering*, 118:50–62.

Capobianco, M., Hanson, H., Larson, M., Steetzel, H., Stive, M. J. F., Chatelus, Y., Aarninkhof, S., and Karambas, T. (2002). Nourishment design and evaluation: applicability of model concepts. *Coastal Engineering*, 47(2):113–135.

Dastgheib, A., Roelvink, J., and Wang, Z. (2008). Long-term process-based morphological modeling of the marsdiep tidal basin. *Marine Geology*, 256(14):90–100.

de Schipper, M. A., de Vries, S., Ruessink, G., de Zeeuw, R. C., Rutten, J., van Gelder-Maas, C., and Stive, M. J. (2016). Initial spreading of a mega feeder nourishment: Observations of the Sand Engine pilot project. *Coastal Engineering*, 111:23–38.

Dong, P., Chen, Y., and Chen, S. (2015). Sediment size effects on rip channel dynamics. *Coastal Engineering*, 99:124–135.

Egiazaroff, I. (1965). Calculation of non-uniform sediment concentrations. *Journal of Hydraulic Division ASCE*, 91(HY4):225–247.

Gallagher, E. L., MacMahan, J. H., Reniers, A. J. H. M., Brown, J. A., and Thornton, E. B. (2011). Grain size variability on a rip-channeled beach. *Marine Geology*, 287:43–53.

Gao, S. and Collins, M. (1992). Net sediment transport patterns inferred from grain-size trends based upon definitions of "transport vectors". *Sedimentary Geology*, 80:47–60.

Geleynse, N., Storms, J. E. A., Walstra, D. J. R., Jagers H R A Wang, Z. B., and Stive, M. J. F. (2011). Controls on river delta formation; insights from numerical modelling. *Earth and Planetary Science Letters*, 302(1-2):217–226.

Giardino, A., Brière, C. D. E., and Van der Werf, J. J. (2011). Morphological modelling of bar dynamics with delft3d. the quest for optimal parameter settings. Technical Report 1202345-000, Deltares.

Gibson, R. N. and Robb, L. (1992). The relationship between body size, sediment grain size and the burying ability of juvenile plaice, pleuronectes platessa l. *Journal of Fish Biology*, 40:771–778.

Grunnet, N. M., Ruessink, B. G., and Walstra, D. J. R. (2005). The influence of tides, wind and waves on the redistribution of nourished sediment at Terschelling, The Netherlands. *Coastal Engineering*, 52(7):617–631.

Guillén, J. and Hoekstra, P. (1996). The "equilibrium" distribtuion of grain size fractions and its implications for cross-shore sediment transport: A conceptual model. *Marine Geology*, 135:15–33.

Guillén, J. and Hoekstra, P. (1997). Sediment Distribution in the Nearshore Zone: Grain Size Evolution in Response to Shoreface Nourishment (Island of Terschelling, The Netherlands). *Estuarine, Coastal and Shelf Science*, 45:639–652.

Holland, K. T. and Elmore, P. A. (2008). A review of heterogeneous sediments in coastal environments. *Earth-Science Reviews*, 89:116–134.

Horn, D. P. (1993). Sediment dynamics on a macrotidal beach, Isle of Man (U.K.). *Journal of Coastal Research*, 9:189–208.

Huisman, B. J. A., De Schipper, M. A., and Ruessink, B. G. (2016). Sediment sorting at the sand motor at storm and annual time scales. *Marine Geology*, 381:209–226.

Inman, D. L. (1953). Areal and seasonal variations in beach and nearshore sediments at La Jolla, California. Technical report, U.S. Army Corps Eng. Beach Erosion Board, Technical Memorandum 39.

Kana, T. W., Rosati, J. D., and Traynum, S. B. (2011). Lack of evidence for onshore sediment transport from deep water at decadal time scales: Fire Island, New York. *Journal of Coastal Research*, SI 59:61–75.

Katoh, K. and Yanagishima, S. (1995). Changes of sand grain distribution in the surf zone. In Zeidler, R. B. and Dally, W. R., editors, *Coastal Dynamics 1995: Proceedings of the International Conference on Coastal Research*, pages 639–650, Gdansk, Poland. Am. Soc. of Civ. Eng.

Knaapen, M. A. F., Holzhauer, H., Hulscher, S. J. M. H., Baptist, M. J., De Vries, M. B., and Van Ledden, M. (2003). On the modelling of biological effects on morphology. *River, Coastal and Estuarine Morphodynamics*, Barcelona:773–783.

Kohsiek, L. (1984). The grain size characteristic of the most seaward range of dimes along the dutch coast (in dutch). Technical Report nota WWKZ-84G.007, Rijkswaterstaat. Dutch title : De korrelgrootte karakteristiek van de zeereep (stuifdijk) langs de Nederlandse kust.

Komar, P. D. (1987). Selective grain entrainment by a current from a bed of mixed sizes: a reanalysis. *Journal of Sedimentary Petrology*, 57 (2):203–211.

Lesser, G. R., Roelvink, J. A., van Kester, J. A. T. M., and Stelling, G. S. (2004). Development and validation of a three-dimensional morphological model. *Coastal Engineering*, 51(8-9):883–915.

Liu, J. T. and Zarillo, G. A. (1987). Partitioning of shoreface sediment grain-sizes. In *Coastal Sediments, New Orleans, USA, pp. 1533–1548.*

Luijendijk, A. P., Ranasinghe, R., de Schipper, M. A., Huisman, B. J. A., Swinkels, C. M., Walstra, D. J. R., and Stive, M. J. F. (2017). The initial morphological response of the Sand Engine: A process-based modelling study. *Coastal Engineering*, 119:1–14.

MacMahan, J., Stanton, T. P., Thornton, E. B., and Reniers, A. J. H. M. (2005). RIPEX-Rip Currents on a shore-connected shoal beach. *Marine Geology*, 218:113–134.

Masselink, G. (1992). Longshore variation of grain-size distribution along the coast of the Rhone Delta, Southern France - a test of the McLaren model. *Journal of Coastal Research*, 8 (2):286 –291.

McLachlan, A. (1996). Physical factors in benthic ecology: Effects of changing sand particle size on beach fauna. *Marine Ecology Progress Series*, 131:205–217.

McLaren, P. A. and Bowles, D. (1985). The effects of sediment transport on grain-size distributions. *Journal of Sedimentary Petrology*, 55:457–470.

Medina, R., Losada, M. A., Losada, I. J., and Vidal, C. (1994). Temporal and spatial relationship between sediment grain size and beach profile. *Marine Geology*, 118 (3):195–206.

Meirelles, S., Henriquez, M., Reniers, A. J. H. M., Luijendijk, A. P., Pietrzak, J. D., Horner-Devine, A. R., Souza, A. J., and Stive, M. J. F. (2017). Cross-shore stratified tidal flow seaward of a mega-nourishment. *Estuarine, Coastal and Shelf Science*.

Moutzouris, C. I., Kraus, N. C., Gingerich, K. J., and Kriebel, D. L. (1991). Beach profiles versus cross-shore distributions of sediment grain sizes. *Advances in Coastal Modeling*, pages 860–874. American Society of Civil Engineers, New York, NY.

Pruszak, Z. (1993). The analysis of beach profile changes using dean's method and empirical orthogonal functions. *Coastal Engineering*, 19:245–261.

Radermacher, M., de Schipper, M. A., Swinkels, C., MacMahan, J. H., and Reniers, A. J. H. M. (2017). Tidal flow separation at protruding beach nourishments. *Journal of Geophysical Research: Oceans*, 122(1):63–79.

Ranasinghe, R., Swinkels, C. M., Luijendijk, A. P., Roelvink, J. A., Bosboom, J., Stive, M. J. F., and Walstra, D. J. R. (2011). Morphodynamic upscaling with the MORFAC approach: Dependencies and sensitivities. *Coastal Engineering*, 58(8):806–811.

Reniers, A. J. H. M., Gallagher, E. L., MacMahan, J. H., Brown, J. A., van Rooijen, A. A., van Thiel de Vries, J. S. M., and van Prooijen, B. C. (2013). Observations and modeling of steep-beach grain-size variability. *Journal of Geophysical Research: Oceans*, 1118 (2):577–591.

Ribberink, J. S. (1987). *Mathematical modelling of onedimensional morphological changes in rivers with nonuniform sediment.* PhD thesis, Delft University of Technology.

Richmond, B. M. and Sallenger, A. H. J. (1984). Cross-shore transport of bimodal sands. *Proceedings of the 19th International Conference on Coastal Engineering*, 2:1997–2008.

Roelvink, J. A. (1993). Dissipation in random wave groups incident on a beach. *Coastal Engineering*, 19:127–150.

Rouse, H. E. (1950). *Engineering hydraulics.* New York, John Wiley and Sons.

Rutten, J., Ruessink, B. G., and Price, T. D. (2017). Observations on sandbar behaviour along a man-made curved coast. *Earth Surface Processes and Landforms*.

Sembiring, L. E., van Ormondt, M., van Dongeren, A. R., and Roelvink, J. A. (2015). A validation of an operational wave and surge prediction system for the Dutch Coast. *Natural Hazards and Earth System Sciences Discussions*, 2:3251–3288.

Sirks, E. E. (2013). Sediment sorting at a large scale nourishment. Master's thesis, Delft University of Technology.

Slingerland, R. and Smith, N. D. (1986). Occurrence and formation of water-laid placers. *Annual Review of Earth and Planetary Sciences*, 14:113–147.

Sloff, C. J., Jagers, H. R. A., Kitamura, Y., and Kitamura, P. (2001). 2d morphodynamic modelling with graded sediment. *Proceedings of 2nd IAHR Symposium on River, Coastal and Estuarine Morphodynamics*, pages 10–14.

Sloff, C. J. and Mosselman, E. (2012). Bifurcation modelling in a meandering gravel–sand bed river. *Earth Surface Processes and Landforms*, 37(14):1556–1566.

Sonu, C. (1972). Bimodal composition and cyclic characteristics of beach sediment in continuously changing profiles. *Journal of Sedimentary Petrology*, 42:852–857.

Stauble, D. K. and Cialone, M. A. (1996). Sediment dynamics and profile interactions: Duck94. *Coastal Engineering*, 4:3921–3934.

Steidtmann, J. R. (1982). Size-density sorting of sand-size spheres during deposition from bedload transport and implications concerning hydraulic equivalence. *Sedimentology*, 29:877–883.

Stive, M. J. F., De Schipper, M. A., Luijendijk, A. P., Aarninkhof, S. G. J., Van Gelder-Maas, C., Van Thiel de Vries, J. S. M., De Vries, S., Henriquez, M., Marx, S., and Ranasinghe, R. (2013). A New Alternative to Saving Our Beaches from Sea-Level Rise: The Sand Engine. *Journal of Coastal Research*, 29 (5):1001–1008.

Terwindt, J. H. J. (1962). Study of grain size variations at the coast of Katwijk 1962 (in Dutch). Report K-324, Rijkswaterstaat, The Hague, The Netherlands.

Van der Zwaag, J. (2014). Development of sediment sorting at the large scale nourishment 'The Sand Motor'. Master's thesis, TU Delft and Deltares. Additional MSc Thesis.

Van Rijn, L. C. (1993). *Principles of sediment transport in Rivers, Estuaries and Coastal Seas*. Aqua publications.

Van Rijn, L. C. (1997). Cross-shore modelling of graded sediments. Technical Report Z2181, WL | Delft Hydraulics.

Van Rijn, L. C. (2007a). Unified View of Sediment Transport by Currents and Waves II: Suspended Transport. *Journal of Hydraulic Engineering*, 133(6):668–689.

Van Rijn, L. C. (2007b). Unified View of Sediment Transport by Currents and Waves III: Graded Beds. *Journal of Hydraulic Engineering*, 133(7):761–775.

Van Rijn, L. C., Walstra, D. J. R., and van Ormondt, M. (2004). Description of TRANSPOR2004 and impelmentation in Delft3D-ONLINE. Report Z3748.00, WL | Delft Hydraulics.

Van Straaten, L. M. J. U. (1965). Coastal barrier deposits in South- and North Holland in particular in the area around Scheveningen and IJmuiden. *Mededelingen van de Geologische Stichting*, 17:41–75.

Visser, A. W., Souza, A. S., Hessner, K., and Simpson, J. H. (1994). The effect of stratification on tidal current profiles in a region of freshwater influence. *Oceanologica Acta*, 17(4):369–381.

Wijnberg, K. M. (2002). Environmental controls on decadal morphologic behaviour of the Holland coast. *Marine Geology*, 189:227–247.

Wilcock, P. R. (1993). Critical shear stress of natural sediments. *Hydraulic Engineering*, 119(4):491–505.

Appendix A. Validation of modelled hydrodynamics

Modelled wave conditions matched well with wave buoy measurements at 11m water depth (x=70.7 and y=451.8 km in RD coordinates) for the 2011-2012 winter period (Figure A.1). Small deviations were noticeable during quiet conditions with wind from land. These mild conditions are, however, not expected to be very relevant for the large-scale morphological changes.

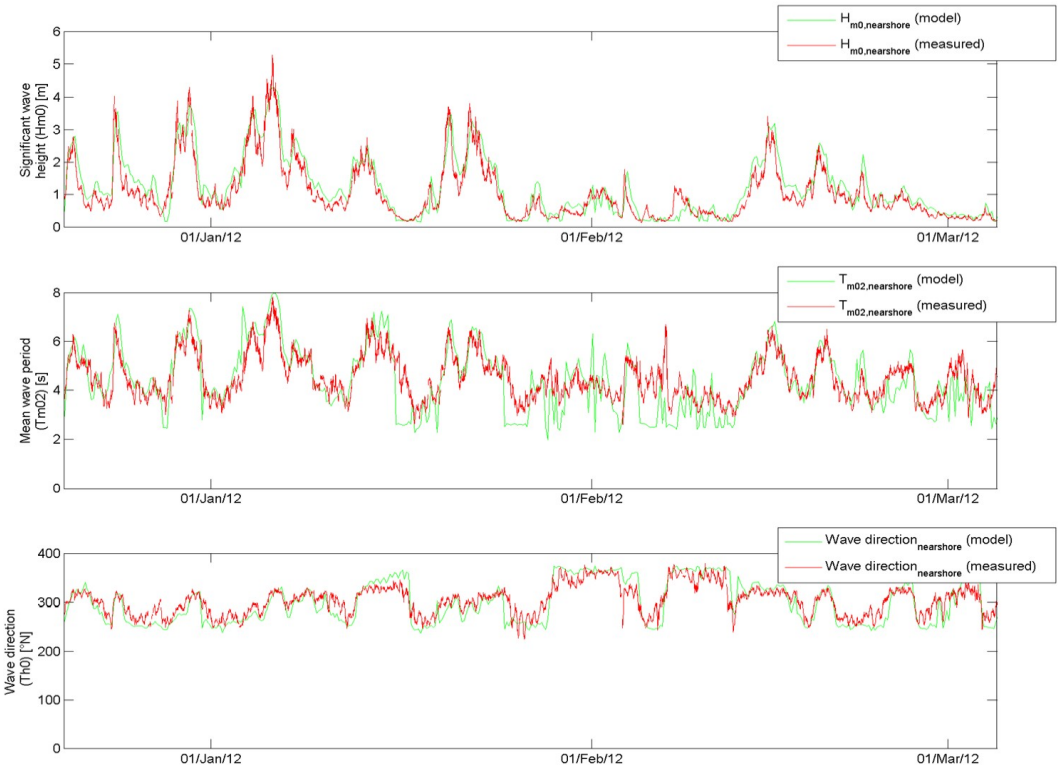

Figure A.1: Computed and measured significant wave height (H_{m0}), period (T_{m02}) and direction at the location of the wave buoy for the 2011-2012 winter period.

Modelled current velocities were validated with measurements at ADCP stations E and F, which were located respectively 1.5 and 3 km North of the Sand Motor (Figure 4) respectively in 5m and 8m water depth in the August 2012 validation period. Reference is also made to Luijendijk et al. (2017) who also validated currents at ADCP F. Current velocities were well represented at both stations (Figure A.2), which provides confidence in the representation of the horizontal tide in the model.

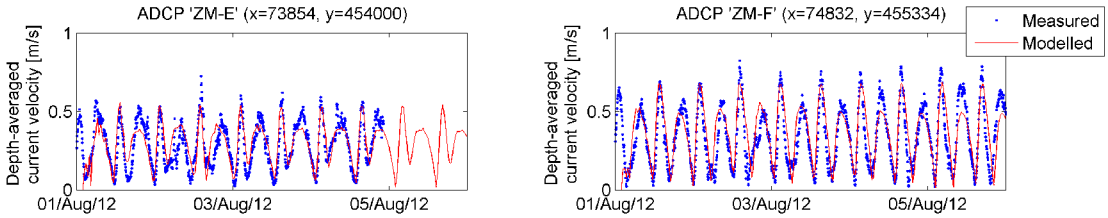

Figure A.2: Computed and measured depth-averaged currents at ADCP stations E (left panel) and F (right panel).